

## 16. COMPOSITION, ALTERATION, AND ORIGIN OF THE BASEMENT LAVAS AND VOLCANICLASTIC ROCKS AT SITE 738, SOUTHERN KERGUELEN PLATEAU<sup>1</sup>

K. W. Mehl,<sup>2</sup> P. R. Bitschene,<sup>2</sup> H.-U. Schmincke,<sup>2</sup> and J. Hertogen<sup>3</sup>

### ABSTRACT

During ODP Leg 119 one basement hole was drilled at Site 738, on the Southern Kerguelen Plateau. The 38.2 m of basement rocks drilled comprises three basaltic aa-lava flows with basal and top breccias, overlain by Turonian marine carbonates. Site 738 basalts probably erupted near a fracture zone, and were emplaced during the plateau-forming stage of Kerguelen Plateau evolution under quiet, subaerial to shallow water conditions.

The basalts are T-MORB, chemically resembling Mesozoic continental flood basalts of the southern hemisphere. Two slightly different magma batches are distinguished by Fe, Ti, Al, Zr, and REE concentrations. Prior to eruption, the magmas had undergone significant olivine and some clinopyroxene fractionation. Incompatible and immobile trace element concentrations and ratios point to a veined upper mantle source, where a refractory mineral assemblage retains Nb, Ta, and the HREE. The basaltic melts derived from this regionally veined, enriched upper mantle have high LREE, and especially Ba and Th concentrations and bear the DUPAL isotopic signature gained from deep-seated, recycled, old oceanic(?) crust.

A saponite-celadonite secondary mineral assemblage confines the alteration temperature to <170°C. Alteration is accompanied by net gains of H<sub>2</sub>O, CO<sub>2</sub>, K<sub>2</sub>O, and Rb, higher oxidation, minor Na<sub>2</sub>O, SiO<sub>2</sub> gains, and losses of V and CaO. Released Ca, together with Ca from seawater, precipitated as calcite in veins and vesicles, plumbed the circulation system and terminated the rock/open seawater interaction.

### INTRODUCTION

The Kerguelen Plateau (46°–64°S) in the southern Indian Ocean is 2500 km long, 600 km wide, and rises 2–4 km above the surrounding ocean floor (Fig. 1). Two Ocean Drilling Program (ODP) legs (119 and 120) were designed to drill a latitudinal transect from Kerguelen Island (49°S) to Prydz Bay (68°S). Major objectives were to study the composition, structure, and age of the Kerguelen basement.

Site 738 (62°42.55'S, 82°47.25'E) lies at the southernmost tip of the Kerguelen Plateau and drilling penetrated 486 m of mostly calcareous, Quaternary through lower Turonian sediments in 2263 m of water. Basement drilling was terminated at 533.8 m below seafloor (mbfs). Core recovery of the basement was 27.2 m or 71%.

The magmatic and volcano-tectonic evolution of the Kerguelen archipelago and the Kerguelen Plateau has recently been outlined by Storey et al. (1988, and literature therein), Bassias et al. (1987), Davies et al. (1989), Schlich, Wise, et al. (1989), and Weis et al. (1989). The following components are considered to contribute to the formation of Kerguelen Plateau basaltic magmas:

1. A depleted, normal (N) mid-ocean ridge basalt (MORB) reservoir.
2. A plume (P) type MORB and ocean island basalt (OIB) reservoir from an enriched, deep mantle source.
3. A highly <sup>87</sup>Sr<sub>rad</sub>-, <sup>208</sup>Pb<sub>rad</sub>-, and <sup>207</sup>Pb<sub>rad</sub>-enriched component derived either from subducted oceanic crust or from old continental lithosphere entrained in the Kerguelen Plateau. This component comes along with the P-MORB type reservoir.

The latter component is responsible for the Sr and Pb isotopic signature of all Kerguelen Plateau magmatic rocks (DUPAL anomaly; Hart, 1984). High Sr- and Pb-isotope ratios (Alibert, this volume) confirm the DUPAL signature of Site 738 basalts. No indication of continental crustal rocks has been found in the basaltic rocks or in the overlying sedimentary sequence. This component, although never confirmed, is still not dismissed when discussing the origin of Kerguelen Plateau basalts (e.g., Davies et al., 1989).

The volcano-tectonic evolution of the southern Kerguelen Plateau (Bitschene et al., 1989) involves:

1. Quiet, subaerial to shallow-water tholeiitic (flood?) basalt volcanism and early rifting (Early to Middle Cretaceous plateau stage);
2. Emplacement, alteration, and erosion of ocean island-type alkali basalt volcanism, major rifting, and foundering (Late Cretaceous seamount stage);
3. Cessation of tectonic and magmatic activity and ongoing subsidence with fully marine conditions since the Paleocene (consolidation and submergence stage); shift of magmatic and tectonic activity toward the northern Kerguelen Plateau.

Site 738 magmatic activity belongs to the plateau-forming stage of Kerguelen Plateau evolution as evidenced by its pre-Turonian age and tholeiitic character.

### METHODS

From fifty-five thin sections studied microscopically, twelve were analyzed by electron microprobe (EMP), using an automated wavelength dispersive system (Cameca). Operating conditions were 15 kV accelerating voltage, 14 and 8 nA beam current for primary and secondary minerals, respectively, and 20 s counting time. Beam diameter was about 8 μm. Na and K were measured first to minimize loss due to volatilization.

Bulk-rock chemical analyses were carried out by X-ray-fluorescence methods (XRF) on glass fusion beads, using an automated Philips PW 1400 spectrometer. The fusion beads consist of rock

<sup>1</sup> Barron, J., Larsen, B., et al., 1991. *Proc. ODP, Sci. Results*, 119: College Station, TX (Ocean Drilling Program).

<sup>2</sup> Institut für Mineralogie, Ruhr-Universität, Postfach 102148, D-4630 Bochum, Federal Republic of Germany.

<sup>3</sup> Katholieke Universiteit, Leuven, Belgium.

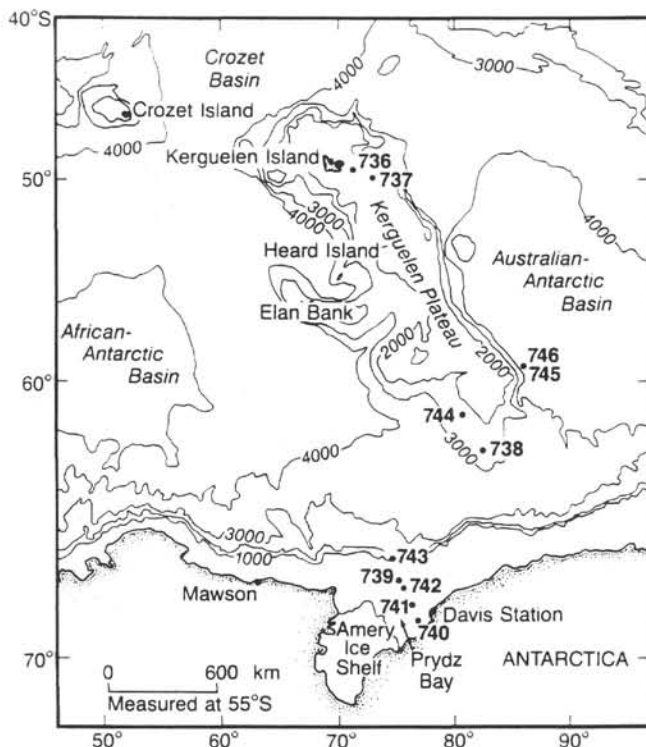


Figure 1. Bathymetric map of Kerguelen Plateau and Prydz Bay with Leg 119 drill sites. Contours in meters. Site 738 basement is studied in this report (from Barron, Larsen, et al., 1989).

powders, dried at 110°C for 24 hr, and flux (lithium metaborate and dilithium tetraborate; Spectromelt, Merck AR) in the ratio 1:4 melted at 1000°C for 20 min and poured into a 34-mm-diameter pellet mold. Precision of the XRF major and trace element data is always better than 3%, except for low Nb (<5 ppm) and Rb (<10 ppm) concentrations, which are near the detection level.

$\text{Fe}^{2+}$  was determined by semiautomatic potentiometric titration of the hydrofluoric acid-silver perchlorate digested sample, with standard potassium bromide solution.

$\text{CO}_2$  was determined by closed-system coulometric titration of barium perchlorate solution, into which the gases were led produced by heating the sample in a tube furnace at 1280°C.

$\text{H}_2\text{O}^+$  was measured by closed-system coulometric titration of a nonaqueous Karl Fischer reagent into which the carrier gas ( $\text{N}_2$ ) was passed, containing water stripped from the sample by heating in a Pt crucible to 1300°C with an induction furnace.

Sample 119-738C-32R-CC, 12–14 cm, was treated with acetic acid for removal of carbonate before whole-rock analysis were carried out.

Only the basaltic clasts were analyzed from Sample 119-738C-32R-CC, 0–4 cm, after being handpicked under a binocular microscope.

Selected trace and rare earth elements (REE) of the freshest whole-rock samples were analyzed by instrumental neutron activation analysis (INAA). The analytical methods were described in detail by Gijbels (1980) and Hertogen and Gijbels (1981).

## RESULTS

### Lithology and Petrography

Basaltic rocks are present in lithostratigraphic Unit VII and make up Unit VIII (Barron, Larsen, et al., 1989). In Subunit VIIa (0.17 m recovery) subangular to rounded basaltic clasts (0.5–>20 mm) are embedded in a bioclastic shallow-water limestone. Subunit VIIb (0.05 m recovery) comprises a fractured and highly vesicular basalt overlain by a micritic limestone containing angular clasts of the underlying

basalt. Large vesicles (about 20%, up to >10 mm long) are rimmed by brown and green sheet silicates and are filled with two generations of carbonate and minor "waxy mass." Fractures are filled by sparry calcite.

The basement (Unit VIII) consists of three massive basalt layers with intercalated breccias (Fig. 2). The lowermost basalt layer (>6.3 m thick) is capped by about 3 m of breccia. The lower half of this breccia is dominated by tachylitic clasts in a dull red basaltic matrix, the upper half by basaltic clasts in a gray matrix. The middle basalt (3.15 m) shows vesicles (3–10 mm in diameter; <15% by volume) at the base and in the top 10 cm. The overlying breccia (2.85 m) comprises mostly vesicular, tachylitic clasts in a red matrix with 0.5 m of massive basalt intercalated in the lower part. The uppermost almost 10-m-thick basalt layer is highly fractured. The brecciated top (1.8 m) grades into the overlying breccia (3.5 m). Mainly basaltic clasts lie in a dull red matrix in the lower 0.9 m of the breccia, whereas in the upper 2.6 m basaltic and tachylitic clasts are embedded in a red to dull red matrix.

The fine-grained basalts vary from grayish red brown to yellowish brown to almost black. They are massive to highly fractured. Narrow fractures are filled by green sheet silicates, and wider ones are rimmed by green sheet silicates and filled by sparry calcite. Vesicles (0%–20%, 0.5–5 mm in diameter, rarely exceeding 20 mm) are filled by various secondary phases. Chilled margins are absent.

The massive basalts have subophitic to intergranular textures. Pegmatoid "schlieren" within the massive basalts (Pl. 1) have dicty-taxitic textures and comprise coarser crystals of plagioclase, clinopyroxene and ore minerals, and altered interstitial glass. Some "schlieren" contain geopetal vesicles filled by dark brown and blue green sheet silicates.

The basalts are aphyric to moderately plagioclase-phyric (0.2–0.9 mm, <5%). Phenocrysts of clinopyroxene (<0.5 mm, <1%) and pseudomorphs of olivine (<0.4 mm, <1%) are area. Fe/Ti-oxides amounts

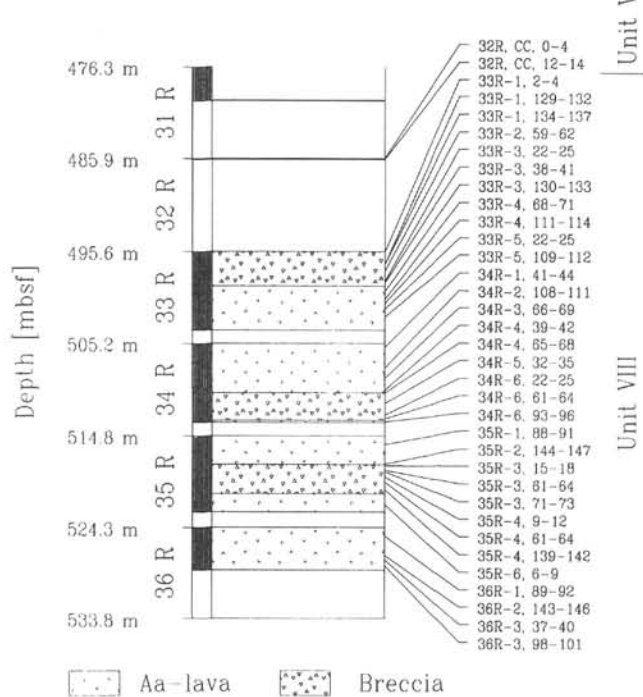


Figure 2. Stratigraphy of Site 738 basement and whole-rock samples studied. Recovery of cores indicated by dark bars.

to 10%–20% (<0.4 mm). The groundmass consists of plagioclase and clinopyroxene microlites in a dark mesostasis.

The breccias comprise mostly rounded to subangular, basaltic clasts (0.5–80 mm, 40%–90% of the total breccia) embedded in a fine-grained, basaltic, highly altered, and varicolored matrix with red to dull red and black, partly green shades. The breccias are unstratified and neither fossils nor terrigenous detritus are mixed or interlayered with the basalt and breccia. Two main types of clasts were distinguished: (1) Tachylitic clasts are gray to brownish black with a tachylitic matrix (about 50%) and a high vesicle content (5%–20%, mostly 1–2 mm in diameter); (2) basaltic clasts are greenish to brown and correspond to the massive basalts. The breccias do not represent hyaloclastic deposits but top breccia (tachylitic clasts) and base breccia (basaltic clasts).

## Chemistry

### Primary Phases

Electron microprobe analyses of plagioclase (Fig. 3 and Table 1 with selected analyses) show variable anorthite (An) content within single samples (e.g., Sample 119-738C-36R-2, 143–146 cm, with An<sub>48</sub>–<sub>73</sub>, microphenocrysts reaching An<sub>48</sub>–<sub>62</sub>, and phenocrysts An<sub>62</sub>–<sub>73</sub>). Plagioclase compositions range from An<sub>69</sub>Ab<sub>30</sub>Or<sub>1</sub> to An<sub>44</sub>Ab<sub>53</sub>Or<sub>3</sub>. Feldspars in two pegmatoid "schlieren" (Pl. 1) show An<sub>61</sub>–<sub>67</sub> (Sample 119-738C-36R-2, 143–146 cm) and An<sub>40</sub>–<sub>49</sub> (Sample 119-738C-33R-5, 30–32 cm). A few plagioclase crystals in Subunit VIIb show oscillatory zoning (e.g., An<sub>68</sub>–An<sub>65</sub>–An<sub>78</sub>–An<sub>59</sub> and An<sub>71</sub>–An<sub>74</sub>–An<sub>65</sub>). The amount of the albite and orthoclase component increases linearly with decreasing An (Fig. 3).

All analyzed pyroxenes are augitic (En<sub>32</sub>–<sub>51</sub>, Fs<sub>8</sub>–<sub>29</sub>, Wo<sub>23</sub>–<sub>35</sub>; Fig. 4 and Table 2 with selected analyses) except for two of pigeonites (Sample 119-738C-36R-2, 143–146 cm: En<sub>64</sub>–<sub>68</sub>, Fs<sub>19</sub>–<sub>24</sub>, Wo<sub>6</sub>–<sub>8</sub>, lowermost two quadrangles in Fig. 4). Some clinopyroxene phenocrysts have high Cr<sub>2</sub>O<sub>3</sub> concentrations (>1%, Table 2).

### Secondary Phases

Secondary phases are dominantly brown and green sheet silicates apart from carbonate. Several phases were distinguished optically and by electron microprobe analysis (Table 3 and Fig. 5).

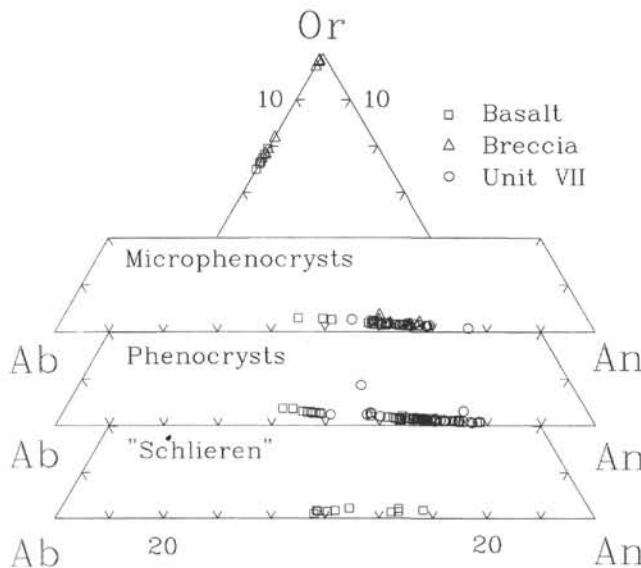


Figure 3. Compositional variation of plagioclase in "pegmatoid schlieren," as phenocrysts and microphenocrysts, and secondary K-feldspar replacing microphenocrysts and glass in the triangle orthoclase(Or)-albite(Ab)-anorthite(An).

Celadonite is microcrystalline to fibrous, some scaly crystals show yellow or grass green to bluish green pleochroism. Celadonite has replaced interstitial glass, plagioclase, and clinopyroxene, and occurs as a major filling of vesicles and veins. Electron microprobe analyses show high iron (17%–25% FeO) and potassium (3%–9.5% K<sub>2</sub>O) concentrations. The analyses have more SiO<sub>2</sub> and less FeO than those reported from Deep Sea Drilling Project (DSDP) Leg 37 (Andrews, 1980).

Green saponite is slightly pleochroic with green to olive green or greenish brown tones. The fibrous, rarely microcrystalline crystals are radially arranged in vesicle fillings and are up to 150 µm long. Green saponites are Mg-rich (18%–20.5% MgO) and low in iron (5.5%–7% FeO) and correspond to the Mg-rich, Fe-poor saponite subgroup of Andrews (1980), but with significantly lower SiO<sub>2</sub> values.

Colorless to coffee brown, fibrous to radially arranged, brown saponite replaces plagioclase and occurs as a minor vesicle filling. The brown saponites have lower MgO (9.5%–17.2%) and higher FeO (9.8%–15.6%) concentrations compared to the green saponites and may correspond to the Fe-rich saponite subgroup of Andrews (1980).

Montmorillonite(?) occurs in two varieties. One variety of montmorillonite (A) is an almost colorless to light brown, nearly isotropic phase and occurs as angular grains in Subunit VIIb (Sample 119-738C-32R-CC, 10–12 cm). The refractive index is <1.54. The material is replaced along the rim and cracks by brown sheet silicates and, along cracks, by calcite.

Electron microprobe analyses show high silica (54%–61% SiO<sub>2</sub>) and alumina (17%–19.2% Al<sub>2</sub>O<sub>3</sub>) contents which fit well the mean composition of 101 montmorillonites-beidellites reported by Weaver and Pollard (1973).

The other montmorillonite(?) variety (B) is cryptocrystalline with various brown shades and concentrically rims and fills vesicles and veins. It was described in Barron, Larsen, et al. (1989) as a "waxy mass." Concentric at vesicle rims, it partly passes over to geopetal vesicle fillings. Some vesicles are completely filled by this phase that generally exhibits shrinkage cracks. Electron microprobe analyses show lower Al (11.5%–17.6%) and higher Mg (7.9%–10.3%) concentrations compared to the mean composition of 101 montmorillonites-beidellites reported by Weaver and Pollard (1973).

Brown sheet silicate phases show various brown colors and are of varying crystallinity (microcrystalline to fibrous). They replace interstitial glass, glass shards, plagioclase and clinopyroxene, line basaltic clasts (Sample 119-738C-32R-CC, 10–12 cm) and phenocrysts in a pegmatoid "schlieren" (Sample 119-738C-34R-4, 39–42 cm), and occur in pseudomorphs after olivine, and as concentric rims and fillings of vesicles and veins.

Calcite replaces plagioclase (especially in the core and along cracks) and interstitial glass. Blocky calcite is a major vesicle- and vein-filling mineral and also occurs in diktytaxitic pegmatoid "schlieren" (e.g., Sample 119-738C-34R-4, 39–42 cm). Vesicle-filling palisade cementation occurs only in Subunit VIIb. Electron microprobe analyses reveal almost pure Ca carbonate. MgO is low (0.3%–1.2%), whereas P<sub>2</sub>O<sub>5</sub> concentrations (0.8%–1.0%) are high and reliable, but cannot readily be explained. Microcrystalline apatite fibers or other phosphate inclusions are suspected to be the reason for the unusual P contents in the calcite. Late stage vesicle-filling calcite contains significant MnO (2.9%–3.6%).

A colorless SiO<sub>2</sub> phase with weak birefringence occurs as round aggregates in vesicles in only one thin section (Sample 119-738C-36R-1, 148–150 cm) and is thought to be chalcedony. Metasomatic SiO<sub>2</sub> replaces carbonate in Subunit VIIa.

Dirty brown, blocky K-feldspar crystals with weak birefringence replace former interstitial glass and also occur in pegmatoid "schlieren," there replacing glassy matrix. Electron microprobe analyses reveal Or<sub>75</sub>–<sub>82</sub> (Table 3) which attributes them a magmatic origin. Microphenocrysts in tachylitic clasts have Or<sub>98</sub>–<sub>99</sub>.

Pseudomorphs after olivine also occur in two types:

**Table 1.** EMP analyses of primary and secondary feldspar of selected Hole 738C samples. Calculations based on O = 32. Remarks: 1 = microphenocryst, 2 = phenocryst, 3 = in "pegmatoid schlieren," 4 = replacing microphenocryst or glass.

Core, Section, Interval [cm]	33R-3 18–120	33R-5 30–32	33R-5 30–32	33R-5 30–32	33R-5 30–32	33R-5 30–32	33R-5 30–32	34R-4 39–42	34R-4 39–42	34R-4 39–42	34R-4 39–42	34R-5 44–46	34R-5 44–46	34R-5 44–46	
Remarks	4	1	1	1	4	4	4	3	3	3	1	1	1	1	1
SiO <sub>2</sub>	63.94	53.56	55.14	53.37	64.54	64.85	65.57	54.98	54.42	55.69	57.49	51.93	52.86	52.38	63.82
TiO <sub>2</sub>	1.03	0.09	0.11	0.07	0.57	0.72	0.29	0.08	0.09	0.09	0.11	0.06	0.07	0.09	0.03
Al <sub>2</sub> O <sub>3</sub>	17.89	28.51	27.13	28.22	17.46	17.67	18.16	27.40	27.74	27.20	26.00	29.42	29.12	29.47	18.52
Fe <sub>2</sub> O <sub>3</sub>	0.00	0.00	0.00	0.00	0.00	0.00	0.00	0.90	0.24	0.19	0.00	0.00	0.00	0.00	0.22
FeO	0.98	1.00	0.98	1.01	1.31	0.74	0.49	0.00	0.57	0.62	0.85	0.71	0.73	0.68	0.00
MnO	0.01	0.00	0.00	0.00	0.02	0.04	0.00	0.06	0.03	0.03	0.02	0.00	0.00	0.01	0.00
MgO	0.00	0.05	0.06	0.09	0.30	0.10	0.03	0.08	0.22	0.10	0.10	0.23	0.23	0.24	0.05
CaO	0.00	11.70	10.09	11.71	0.00	0.00	0.00	9.73	10.87	9.77	8.76	13.12	12.83	13.07	0.00
Na <sub>2</sub> O	1.91	4.46	5.29	4.42	2.48	2.37	2.20	5.84	5.00	5.70	5.95	3.83	3.77	3.40	0.28
K <sub>2</sub> O	13.29	0.28	0.45	0.36	12.10	12.89	12.93	0.18	0.37	0.27	0.50	0.20	0.28	0.37	16.44
SrO	nd	nd	nd	nd	nd	nd	nd	nd	nd	nd	nd	nd	nd	nd	nd
Total	99.05	99.65	99.24	99.24	98.78	99.38	99.66	99.24	99.55	99.66	99.78	99.50	99.90	99.71	99.37
Si	11.92	9.75	10.03	9.75	12.02	12.00	12.09	9.97	9.88	10.06	10.38	9.48	9.63	9.57	11.88
Ti	0.14	0.01	0.02	0.01	0.08	0.10	0.04	0.01	0.01	0.01	0.01	0.01	0.01	0.01	0.00
Al	3.93	6.11	5.82	6.08	3.83	3.85	3.95	5.86	5.93	5.79	5.53	6.33	6.25	6.35	4.06
Fe <sup>3+</sup>	0.00	0.00	0.00	0.00	0.00	0.00	0.00	0.12	0.03	0.03	0.00	0.00	0.00	0.00	0.03
Fe <sup>2+</sup>	0.15	0.15	0.15	0.15	0.20	0.11	0.08	0.00	0.09	0.09	0.13	0.11	0.11	0.10	0.00
Mn	0.00	0.00	0.00	0.00	0.00	0.01	0.00	0.01	0.01	0.00	0.00	0.00	0.00	0.00	0.00
Mg	0.00	0.01	0.02	0.02	0.08	0.03	0.01	0.02	0.06	0.03	0.03	0.06	0.06	0.07	0.01
Ca	0.00	2.28	1.97	2.29	0.00	0.00	0.00	1.89	2.11	1.89	1.69	2.57	2.50	2.56	0.00
Na	0.69	1.58	1.87	1.57	0.89	0.85	0.79	2.05	1.76	2.00	2.08	1.36	1.33	1.21	0.10
K	3.16	0.07	0.10	0.08	2.87	3.04	3.04	0.04	0.09	0.06	0.12	0.05	0.06	0.09	3.90
Sr	nd	nd	nd	nd	nd	nd	nd	nd	nd	nd	nd	nd	nd	nd	nd
Sum Z	15.85	15.86	15.85	15.83	15.85	15.85	16.03	15.82	15.81	15.85	15.91	15.81	15.88	15.92	15.94
Sum X	3.85	3.92	3.94	3.94	3.77	3.89	3.83	3.98	3.96	3.95	3.89	3.97	3.90	3.85	4.01
Or	82.06	1.66	2.64	2.11	76.26	78.18	79.42	1.04	2.19	1.57	2.98	1.15	1.66	2.26	97.45
Ab	17.94	40.16	47.39	39.74	23.74	21.82	20.58	51.53	44.43	50.55	53.49	34.20	34.16	31.30	2.55
An	0.00	58.17	49.97	58.15	0.00	0.00	0.00	47.44	53.37	47.88	43.53	64.66	64.18	66.44	0.00

Type I comprises irregularly oriented, fibrous, brown sheet silicates with a slightly anisotropic, colorless, microcrystalline mineral (probably a SiO<sub>2</sub> phase) near the center. An irregular cleavage is characteristic. Anhedral opaque minerals may be embedded in the center and/or they are accumulated at the rim.

Type II is colorless to faintly greenish pleochroic to dark orange, the latter being caused by an increasing amount of Fe (up to >50% FeO; cf. Table 3). The orange variety differs from iddingsite (Deer et al., 1982) by significant lower MgO concentrations. The colorless variety has significant iron (10.3%–18% FeO) and relatively low silicon (40.2%–48.7% SiO<sub>2</sub>) contents. Most pseudomorphs are strongly "cleaved" and show almost parallel extinction and high birefringence and may correspond to type IV "iddingsite" of Baker and Haggerty (1967).

The compositions of typical vesicle filling phases (Fig. 6) were analyzed by electron microprobe from rim to core for two parageneses (Fig. 7). Paragenesis B ("waxy mass"-light brown sheet mineral-green saponite-calcite) shows increasing concentrations of FeO and MgO and decreasing K<sub>2</sub>O, Na<sub>2</sub>O, Al<sub>2</sub>O<sub>3</sub>, and SiO<sub>2</sub>. The pattern of paragenesis A (varicolored sheet silicates, see Figs. 6A and 7) is dominated by the precipitation of celadonite (= bright green) with a maximum of K<sub>2</sub>O and minimum of CaO and MgO. CaO and Na<sub>2</sub>O generally decrease from rim to core whereas FeO shows ambiguous behavior.

### Bulk Rock

All values, graphs, and interpretations of bulk rock chemistry (Table 4, Figs. 8, 9, 10) are based on normalized, volatile-free calcu-

lations, except for the Rare Earth Elements (REE, Fig. 11). The microscopically and chemically freshest basalt samples (119-738C-34R-2, 108–111 cm; 119-738C-36R-2, 143–146 cm; 119-738C-36R-3, 37–40 cm; 119-738C-36R-3, 98–101 cm) have the lowest H<sub>2</sub>O (0.75%–1.32%), CO<sub>2</sub> (0.06%–0.12%), and Fe<sub>2</sub>O<sub>3</sub>/FeO (0.45%–0.59%), and low K<sub>2</sub>O (0.38%–1.10%) and Rb (5–27 ppm) concentrations. Their K/Rb ratios lie between 166 and 307, whereas altered samples have much higher K/Rb ratios (e.g., Sample 119-738C-34R-6, 61–64 cm: 2550). The fresh samples are used when discussing source characteristics of the basaltic suite. Ratios of alteration-insensitive elements (Zr, Nb, Ta, Ti, REE, Cr) from all samples further constrain the source region and, together with normalized absolute concentrations of alteration-insensitive elements, help to explain small intraflow and intrasuite variations.

### Classification

On a normative basis, the freshest samples are olivine-free, hypersthene- normative quartz-tholeiites with high normative orthoclase and albite (Tables 1 and 5). The tholeiitic character is substantiated by the presence of Mg-rich and Mg-poor clinopyroxene (Table 4). The freshest samples also plot into the tholeiitic field within a K<sub>2</sub>O + Na<sub>2</sub>O vs. SiO<sub>2</sub> diagram (e.g., MacDonald and Katsura, 1964). High Fe<sup>+++</sup>, Ca loss, and K gain of the altered rocks do not allow proper norm calculations or TAS plots of all basement samples. But all samples are considered to be originally quartz-tholeiitic basalts on grounds of the close relationship in incompatible and immobile element concentrations, and the spatial coherence.

Table 1. (continued).

Core, Section, Interval [cm]	34R-5 44-46	34R-5 44-46	35R-3 15-18	36R-1 48-150	36R-1 48-150	36R-1 48-150	36R-2 43-146							
Remarks	1	1	1	2	2	2	3	3	2	2	1	1	1	1
SiO <sub>2</sub>	52.68	64.38	54.08	52.05	52.37	51.07	52.71	51.78	53.79	51.11	52.58	55.29	52.60	53.87
TiO <sub>2</sub>	0.05	0.01	0.09	0.06	0.07	0.05	0.04	0.12	0.13	0.00	0.06	0.11	0.21	0.03
Al <sub>2</sub> O <sub>3</sub>	28.97	18.53	27.86	29.07	29.22	30.29	28.03	22.14	27.53	29.16	28.03	26.15	27.99	27.63
FeO	0.00	0.22	0.00	0.43	0.11	0.00	1.06	4.26	0.82	0.58	0.56	0.90	0.10	0.66
MnO	0.02	0.01	0.00	0.01	0.04	0.03	0.00	0.10	0.05	0.02	0.06	0.04	0.05	0.02
MgO	0.24	0.02	0.15	0.11	0.09	0.17	0.14	2.81	0.09	0.21	0.21	0.03	0.06	0.09
CaO	12.83	0.00	11.50	12.91	12.91	13.90	12.80	13.37	12.02	14.26	12.88	10.00	12.71	11.91
Na <sub>2</sub> O	3.71	0.14	4.18	4.06	4.03	3.43	4.26	3.39	4.71	3.40	4.13	5.61	4.08	4.51
K <sub>2</sub> O	0.22	16.87	0.46	0.22	0.25	0.15	0.24	0.30	0.35	0.17	0.26	0.49	0.28	0.42
SrO	nd	nd	nd	nd	nd	nd	0.29	0.32	0.25	0.30	0.27	0.29	0.38	0.32
Total	99.40	100.19	99.30	99.32	99.82	99.58	99.57	98.59	99.74	99.22	99.04	98.91	99.10	99.83
Si	9.64	11.90	9.92	9.52	9.53	9.33	9.65	9.69	9.80	9.42	9.67	10.11	9.69	9.83
Ti	0.01	0.00	0.01	0.01	0.01	0.01	0.01	0.02	0.02	0.00	0.01	0.02	0.03	0.00
Al	6.25	4.04	6.02	6.27	6.26	6.52	6.05	4.88	5.91	6.33	6.08	5.64	6.08	5.94
Fe <sup>3+</sup>	0.00	0.03	0.00	0.06	0.01	0.00	0.15	0.60	0.11	0.08	0.08	0.12	0.01	0.09
Fe <sup>2+</sup>	0.11	0.00	0.15	0.06	0.11	0.08	0.00	0.00	0.00	0.00	0.00	0.00	0.10	0.06
Mn	0.00	0.00	0.00	0.00	0.01	0.00	0.00	0.02	0.01	0.00	0.01	0.01	0.01	0.00
Mg	0.06	0.01	0.04	0.03	0.03	0.05	0.04	0.78	0.02	0.06	0.06	0.01	0.02	0.02
Ca	2.52	0.00	2.26	2.53	2.52	2.72	2.51	2.68	2.35	2.82	2.54	1.96	2.51	2.33
Na	1.31	0.05	1.49	1.44	1.42	1.21	1.51	1.23	1.66	1.22	1.47	1.99	1.46	1.60
K	0.05	3.98	0.11	0.05	0.06	0.03	0.06	0.07	0.08	0.04	0.06	0.11	0.07	0.10
Sr	nd	nd	nd	nd	nd	nd	0.03	0.03	0.03	0.03	0.03	0.03	0.04	0.03
Sum Z	15.89	15.93	15.78	15.79	15.85	15.70	14.57	15.72	15.75	15.75	15.75	15.76	15.77	
Sum X	3.88	4.03	3.85	4.02	4.00	3.97	4.08	3.98	4.09	4.07	4.07	4.06	4.03	4.02
Or	1.31	98.76	2.79	1.29	1.43	0.86	1.37	1.80	1.99	0.98	1.50	2.81	1.63	2.43
Ab	33.87	1.24	38.57	35.79	35.60	30.58	37.07	30.89	40.66	29.85	36.17	48.96	36.15	39.67
An	64.82	0.00	58.64	62.91	62.97	68.56	61.55	67.32	57.35	69.17	62.33	48.23	62.22	57.90

**Element Variation with Depth**

Some elements show considerable variations when basalts and volcaniclastics are considered (Fig. 8), e.g., Cr (51–237 ppm), Ba (119–517 ppm), Ni (24–82 ppm), Cu (23–173 ppm), Rb (5–47 ppm), and Y (24–58 ppm). Other elements have rather similar concentrations, e.g., SiO<sub>2</sub> (47.07–53.34%), TiO<sub>2</sub> (1.42–2.27%), and Zr (128–197 ppm).

Cr (Fig. 8, Table 6) averages 94 ± 43 ppm for the samples below 497 mbsf, and then rises abruptly to 237 ppm in the top basaltic flow and volcaniclastic unit at 495.5–497 mbsf. Ni decreases slightly with depth. The alkali metals Rb, K, and Na, as well as Al are also roughly negatively correlated with depth. In general, the clastic and brecciated rocks are the most sensitive for alteration and display larger scatter in element concentrations than the basalts which dominate the section below 521 mbsf.

**Element Variation with ZR as Differentiation Index**

Zr is used as differentiation index (Fig. 9) as alteration may have led to variations in MgO unrelated to differentiation processes. The basalt flow samples (quadrangles in Fig. 9) show positive correlations of TiO<sub>2</sub>, Al<sub>2</sub>O<sub>3</sub>, Na<sub>2</sub>O, V, and Sr with Zr. Cr, SiO<sub>2</sub>, and P<sub>2</sub>O<sub>5</sub>, and, with a larger scatter, Nb, Ba, and Ni have rather constant levels at different Zr concentrations. All other (alteration sensitive) elements show a large scatter with Zr, similar to the scatter shown by the breccias.

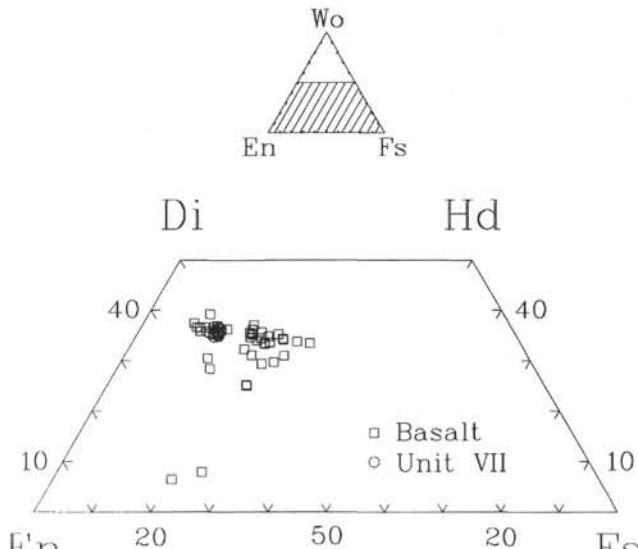


Figure 4. Chemical composition of clinopyroxenes in the quadrilateral enstatite(En)-ferrosilite(Fs)-hedenbergite(Hd)-diopside(Di).

Table 2. EMP analyses of clinopyroxene of selected Hole 738C samples. Calculations based on O = 6.

Core, Section, Interval [cm]	33R-1 2–4	33R-1 2–4	33R-1 4–4	33R-1 2–4	33R-5 30–32	33R-5 30–32	34R-4 39–42	36R-1 148– 150
SiO <sub>2</sub>	51.28	49.31	51.22	50.15	48.90	49.26	50.56	50.50
TiO <sub>2</sub>	0.40	0.93	0.47	0.74	1.02	0.99	0.85	0.76
Al <sub>2</sub> O <sub>3</sub>	2.00	3.21	2.12	3.07	1.57	1.30	2.18	1.95
Fe <sub>2</sub> O <sub>3</sub>	1.52	2.98	1.65	2.04	2.87	2.53	1.39	1.11
FeO	5.58	5.51	5.26	7.86	13.75	14.03	13.67	11.39
MnO	0.25	0.25	0.19	0.30	0.42	0.49	0.33	0.26
MgO	17.33	15.52	17.33	17.44	12.71	12.88	16.84	14.88
CaO	18.61	19.59	18.76	15.92	16.66	16.52	12.96	17.47
Na <sub>2</sub> O	0.23	0.27	0.27	0.19	0.25	0.23	0.20	0.27
K <sub>2</sub> O	0.00	0.01	0.01	0.01	0.00	0.01	0.04	0.02
Cr <sub>2</sub> O <sub>3</sub>	1.04	0.57	1.15	0.42	0.00	0.03	0.00	0.05
Total	98.23	98.16	98.42	98.14	98.16	98.29	99.02	98.65
Si	1.92	1.86	1.91	1.88	1.90	1.91	1.91	1.91
Ti	0.01	0.03	0.01	0.02	0.03	0.03	0.02	0.02
Al	0.09	0.14	0.09	0.14	0.07	0.06	0.10	0.09
Fe <sup>3+</sup>	0.04	0.08	0.05	0.06	0.08	0.07	0.04	0.03
Fe <sup>2+</sup>	0.17	0.17	0.16	0.25	0.45	0.46	0.43	0.36
Mn	0.01	0.01	0.01	0.01	0.01	0.02	0.01	0.01
Mg	0.97	0.87	0.96	0.98	0.74	0.75	0.95	0.84
Ca	0.75	0.79	0.75	0.64	0.69	0.69	0.52	0.71
Na	0.02	0.02	0.02	0.01	0.02	0.02	0.01	0.02
K	0.00	0.00	0.00	0.00	0.00	0.00	0.00	0.00
Cr	0.03	0.02	0.03	0.01	0.00	0.00	0.00	0.00
Enstatite	48.26	43.66	48.16	48.81	36.82	37.28	47.30	41.95
Ferrosilite	9.11	9.09	8.51	12.82	23.04	23.60	22.06	18.42
Wollastonite	32.80	34.00	32.66	26.94	31.29	31.45	23.17	32.91
Core, Section, Interval [cm]	36R-1 148–150	36R-1 148–150	36R-2 143–146	36R-2 143–146	36R-2 143–146	36R-2 143–146	36R-2 143–146	36R-2 143–146
SiO <sub>2</sub>	49.96	49.82	51.54	53.31	51.42	51.81	52.03	50.71
TiO <sub>2</sub>	0.85	0.97	0.68	0.38	0.74	1.05	0.56	0.86
Al <sub>2</sub> O <sub>3</sub>	1.99	1.97	1.41	0.83	1.62	2.01	1.79	1.49
Fe <sub>2</sub> O <sub>3</sub>	1.11	1.49	1.53	1.97	3.25	2.35	2.38	2.23
FeO	13.35	12.78	11.53	14.95	8.60	9.15	7.50	13.03
MnO	0.35	0.32	0.30	0.43	0.13	0.31	0.17	0.23
MgO	14.08	13.85	16.13	23.52	16.14	18.61	16.84	14.47
CaO	16.57	17.05	16.24	4.91	18.40	14.90	18.81	16.74
Na <sub>2</sub> O	0.23	0.30	0.14	0.06	0.20	0.19	0.18	0.15
K <sub>2</sub> O	0.02	0.01	0.00	0.00	0.01	0.03	0.00	0.02
Cr <sub>2</sub> O <sub>3</sub>	0.02	0.00	nd	nd	nd	nd	nd	nd
Total	98.52	98.56	99.50	100.36	100.51	100.42	100.26	99.93
Si	1.91	1.90	1.93	1.95	1.91	1.90	1.92	1.92
Ti	0.02	0.03	0.02	0.01	0.02	0.03	0.02	0.02
Al	0.09	0.09	0.06	0.04	0.07	0.09	0.08	0.07
Fe <sup>3+</sup>	0.03	0.04	0.04	0.05	0.09	0.07	0.07	0.06
Fe <sup>2+</sup>	0.43	0.41	0.36	0.46	0.27	0.28	0.23	0.41
Mn	0.01	0.01	0.01	0.01	0.00	0.01	0.01	0.01
Mg	0.80	0.79	0.90	1.28	0.89	1.02	0.93	0.82
Ca	0.68	0.70	0.65	0.19	0.73	0.59	0.74	0.68
Na	0.02	0.02	0.01	0.00	0.01	0.01	0.01	0.01
K	0.00	0.00	0.00	0.00	0.00	0.00	0.00	0.00
Cr	0.00	0.00	nd	nd	nd	nd	nd	nd
Enstatite	40.06	39.45	45.09	64.01	44.59	50.93	46.29	40.76
Ferrosilite	21.89	20.93	18.56	23.49	13.53	14.53	11.84	20.96
Wollastonite	31.31	32.17	30.25	7.47	32.88	25.88	33.89	30.95

**Table 3.** EMP analyses of sheet silicates of selected Hole 738C samples. Calculations based on O = 22 and iron as Fe<sup>2+</sup>. 1–9 = celadonite, 10–14 = green saponite, 15–24 = brown saponite, 25–38 = ?montmorillonite, 39–44 = various brown sheet silicates, 45–47 = olivine-pseudomorphs.

Core, Section, Interval [cm]	1	2	3	4	5	6	7	8	9	10	11	12
	32R-CC 10–12	32R-CC 10–12	32R-CC 10–12	32R-CC 10–12	33R-1 2–4	33R-1 2–4	33R-1 2–4	33R-5 30–32	36R-1 148–150	34R-5 32–35	34R-5 44–46	34R-5 44–46
SiO <sub>2</sub>	54.00	51.53	47.27	52.65	54.21	53.99	54.06	54.53	51.23	40.22	46.63	46.39
TiO <sub>2</sub>	0.00	0.02	0.04	0.17	0.09	0.07	0.17	0.06	0.08	0.06	0.00	0.02
Al <sub>2</sub> O <sub>3</sub>	5.24	3.62	3.28	7.02	3.40	2.84	3.20	2.08	2.93	6.08	7.45	7.45
FeO	19.84	24.86	14.73	18.34	17.14	17.86	17.31	18.96	17.17	6.87	7.81	7.88
MnO	0.03	0.00	0.01	0.01	0.03	0.04	0.00	0.05	0.00	0.12	0.08	0.14
MgO	5.33	4.00	4.88	7.87	6.40	6.29	6.70	7.19	8.92	19.65	24.69	24.36
CaO	0.58	0.30	0.17	0.63	0.23	0.23	0.23	0.00	0.00	1.21	0.40	0.36
Na <sub>2</sub> O	0.06	0.05	0.08	0.17	0.07	0.01	0.06	0.00	0.01	0.97	0.17	0.16
K <sub>2</sub> O	5.22	6.77	7.29	3.03	9.41	9.28	9.29	9.68	7.38	0.54	0.04	0.05
Total	90.30	91.15	77.75	89.89	90.98	90.61	91.02	92.55	87.71	75.72	87.27	86.82
Si	8.15	8.04	8.33	7.84	8.24	8.27	8.22	8.23	8.04	6.86	6.81	6.82
AlIV	0.00	0.00	0.00	0.16	0.00	0.00	0.00	0.00	0.00	1.14	1.19	1.18
Total	8.15	8.04	8.33	8.00	8.24	8.27	8.22	8.23	8.04	8.00	8.00	8.00
AlVI	0.93	0.67	0.68	1.07	0.61	0.51	0.57	0.37	0.54	0.08	0.09	0.11
Ti	0.00	0.00	0.01	0.02	0.01	0.01	0.02	0.01	0.01	0.01	0.00	0.00
Fe <sup>2+</sup>	2.50	3.25	2.17	2.28	2.18	2.29	2.20	2.39	2.25	0.98	0.95	0.97
Mn	0.00	0.00	0.00	0.00	0.00	0.01	0.00	0.01	0.00	0.02	0.01	0.02
Mg	1.20	0.93	1.28	1.75	1.45	1.44	1.52	1.62	2.09	5.00	5.38	5.34
Total	4.64	4.84	4.14	5.12	4.25	4.25	4.31	4.40	4.89	6.08	6.43	6.44
Ca	0.09	0.05	0.03	0.10	0.04	0.04	0.04	0.00	0.00	0.22	0.06	0.06
Na	0.02	0.02	0.03	0.05	0.02	0.00	0.02	0.00	0.00	0.32	0.05	0.04
K	1.00	1.35	1.64	0.58	1.82	1.81	1.80	1.86	1.48	0.12	0.01	0.01
Total	1.12	1.41	1.70	0.72	1.88	1.85	1.86	1.86	1.48	0.66	0.12	0.11
Core, Section, Interval [cm]	13	14	15	16	17	18	19	20	21	22	23	24
	34R-5 44–46	34R-5 44–46	33R-1 2–4	33R-1 2–4	33R-3 118–120	33R-3 118–120	33R-3 118–120	33R-3 118–120	33R-5 30–32	33R-5 30–32	33R-5 30–32	36R-1 148–150
SiO <sub>2</sub>	46.15	44.46	44.34	46.40	47.38	47.83	47.15	47.76	46.37	46.42	47.63	44.24
TiO <sub>2</sub>	0.03	0.02	0.02	0.23	0.13	0.16	0.02	0.15	0.05	0.11	0.08	0.07
Al <sub>2</sub> O <sub>3</sub>	7.20	6.80	7.21	8.36	7.28	6.50	5.76	6.87	7.37	7.44	6.72	4.63
FeO	7.79	8.66	15.57	13.10	17.94	19.09	12.00	19.16	17.00	18.32	17.20	16.13
MnO	0.30	0.11	0.04	0.05	0.02	0.07	0.05	0.02	0.04	0.05	0.11	0.05
MgO	23.40	22.35	12.36	9.58	14.90	12.43	20.04	13.25	17.06	16.08	15.28	16.28
CaO	2.39	0.74	1.76	1.52	0.86	0.72	0.38	0.89	0.98	1.01	1.03	0.60
Na <sub>2</sub> O	0.22	0.49	0.49	0.40	0.41	0.39	0.13	0.47	0.26	0.29	0.33	0.12
K <sub>2</sub> O	0.05	0.04	0.69	0.79	0.75	1.63	0.70	1.12	0.36	0.53	1.00	0.46
Total	87.53	83.66	82.48	80.43	89.67	88.82	86.23	89.67	89.49	90.24	89.37	82.58
Si	6.78	6.84	7.19	7.52	7.09	7.29	7.13	7.20	6.93	6.93	7.15	7.18
AlIV	1.22	1.16	0.81	0.48	0.91	0.71	0.87	0.80	1.07	1.07	0.85	0.82
Total	8.00	8.00	8.00	8.00	8.00	8.00	8.00	8.00	8.00	8.00	8.00	8.00
AlVI	0.03	0.07	0.56	1.12	0.37	0.46	0.15	0.42	0.23	0.24	0.34	0.06
Ti	0.00	0.00	0.00	0.03	0.01	0.02	0.00	0.02	0.01	0.01	0.01	0.01
Fe <sup>2+</sup>	0.96	1.11	2.11	1.78	2.25	2.43	1.52	2.42	2.13	2.29	2.16	2.19
Mn	0.04	0.01	0.01	0.01	0.00	0.01	0.01	0.00	0.01	0.01	0.01	0.01
Mg	5.13	5.12	2.99	2.31	3.32	2.82	4.51	2.98	3.80	3.58	3.42	3.94
Total	6.15	6.33	5.67	5.24	5.96	5.75	6.19	5.84	6.17	6.13	5.94	6.20
Ca	0.38	0.12	0.31	0.26	0.14	0.12	0.06	0.14	0.16	0.16	0.17	0.10
Na	0.06	0.15	0.15	0.13	0.12	0.12	0.04	0.14	0.07	0.08	0.10	0.04
K	0.01	0.01	0.14	0.16	0.14	0.32	0.13	0.21	0.07	0.10	0.19	0.09
Total	0.45	0.28	0.60	0.55	0.40	0.55	0.23	0.49	0.30	0.34	0.45	0.24

Table 3. (continued).

Core, Section, Interval [cm]	25	26	27	28	29	30	31	32	33	34	35	36
	32R-CC 10–12	32R-CC 10–12	32R-CC 10–12	32R-CC 10–12	32R-CC 10–12	34R-5 44–46	34R-5 44–46	34R-5 44–46	34R-5 44–46	34R-5 44–46	34R-5 44–46	34R-5 44–46
SiO <sub>2</sub>	61.08	59.37	59.80	59.02	61.10	60.53	56.55	56.46	61.79	56.83	60.31	57.89
TiO <sub>2</sub>	0.26	0.77	0.93	0.79	0.47	0.46	0.90	0.78	0.36	1.55	0.60	0.38
Al <sub>2</sub> O <sub>3</sub>	17.47	19.20	18.46	17.79	18.19	16.49	14.68	13.86	17.64	13.43	17.12	14.51
FeO	3.80	3.00	3.79	4.98	2.96	4.11	5.72	6.43	2.59	6.75	3.69	5.17
MnO	0.07	0.00	0.10	0.14	0.11	0.06	0.10	0.07	0.04	0.16	0.05	0.04
MgO	6.99	5.91	5.84	5.88	6.92	8.88	8.42	9.21	8.82	9.71	7.90	10.37
CaO	0.89	0.98	0.89	0.83	0.96	0.71	2.36	1.50	0.77	1.58	0.58	1.09
Na <sub>2</sub> O	0.18	0.16	0.28	0.26	0.15	0.38	0.94	0.87	0.29	1.14	0.56	0.65
K <sub>2</sub> O	1.00	0.75	1.38	1.48	1.15	1.56	2.89	2.93	1.43	2.90	2.51	2.13
Total	91.74	90.14	91.47	91.17	92.01	93.19	92.55	92.11	93.71	94.04	93.30	92.22
Si	7.96	7.83	7.85	7.83	7.91	7.84	7.61	7.65	7.87	7.57	7.82	7.71
AllV	0.04	0.17	0.15	0.17	0.09	0.16	0.39	0.35	0.13	0.43	0.18	0.29
Total	8.00	8.00	8.00	8.00	8.00	8.00	8.00	8.00	8.00	8.00	8.00	8.00
AlVI	2.64	2.81	2.70	2.61	2.69	2.35	1.94	1.86	2.52	1.68	2.44	1.99
Ti	0.03	0.08	0.09	0.08	0.05	0.04	0.09	0.08	0.03	0.15	0.06	0.04
Fe <sup>2+</sup>	0.41	0.33	0.42	0.55	0.32	0.44	0.64	0.73	0.28	0.75	0.40	0.58
Mn	0.01	0.00	0.01	0.02	0.01	0.01	0.01	0.01	0.00	0.02	0.01	0.00
Mg	1.36	1.16	1.14	1.16	1.34	1.71	1.69	1.86	1.67	1.93	1.53	2.06
Total	4.45	4.38	4.36	4.42	4.40	4.56	4.37	4.54	4.51	4.53	4.43	4.66
Ca	0.12	0.14	0.13	0.12	0.13	0.10	0.34	0.22	0.11	0.23	0.08	0.15
Na	0.05	0.04	0.07	0.07	0.04	0.10	0.24	0.23	0.07	0.29	0.14	0.17
K	0.17	0.13	0.23	0.25	0.19	0.26	0.50	0.51	0.23	0.49	0.41	0.36
Total	0.34	0.31	0.43	0.44	0.36	0.45	1.08	0.95	0.41	1.01	0.64	0.69
Core, Section, Interval [cm]	37	38	39	40	41	42	43	44	45	46	47	
	34R-5 44–46	34R-5 44–46	32R-CC 10–12	32R-CC 10–12	32R-CC 10–12	32R-CC 10–12	36R-1 148–150	36R-1 148–150	35R-3 15–18	35R-3 15–18	35R-3 15–18	
SiO <sub>2</sub>	58.35	58.02	57.77	57.75	56.66	52.67	58.97	57.73	40.19	48.65	46.68	
TiO <sub>2</sub>	0.48	0.35	0.43	0.07	0.11	0.08	0.45	0.26	0.76	0.43	0.29	
Al <sub>2</sub> O <sub>3</sub>	15.35	14.80	14.52	13.30	9.75	8.30	13.24	11.92	9.86	7.83	8.49	
FeO	4.82	5.26	10.48	10.19	14.19	16.67	7.01	7.59	18.07	13.02	10.36	
MnO	0.08	0.16	0.02	0.05	0.02	0.00	0.08	0.00	0.02	0.06	0.01	
MgO	8.53	10.22	5.99	7.02	8.31	9.49	9.22	9.60	4.70	5.95	6.22	
CaO	0.91	1.22	1.03	0.99	0.91	0.74	0.92	0.86	0.71	1.03	0.85	
Na <sub>2</sub> O	0.53	0.61	0.21	0.14	0.11	0.37	0.28	0.27	1.03	1.01	0.83	
K <sub>2</sub> O	2.24	1.84	1.11	0.96	0.61	1.54	1.01	1.26	1.29	1.35	1.20	
Total	91.28	92.49	91.56	90.47	90.67	89.86	91.17	89.48	76.63	79.33	74.93	
Si	7.81	7.70	7.87	7.94	7.97	7.71	7.93	7.96	7.15	7.96	7.95	
AllV	0.19	0.30	0.13	0.06	0.03	0.29	0.07	0.04	0.85	0.04	0.05	
Total	8.00	8.00	8.00	8.00	8.00	8.00	8.00	8.00	8.00	8.00	8.00	
AlVI	2.24	2.02	2.20	2.10	1.58	1.14	2.02	1.89	1.22	1.46	1.65	
Ti	0.05	0.03	0.04	0.01	0.01	0.01	0.05	0.03	0.10	0.05	0.04	
Fe <sup>2+</sup>	0.54	0.58	1.19	1.17	1.67	2.04	0.79	0.87	2.69	1.78	1.47	
Mn	0.01	0.02	0.00	0.01	0.00	0.00	0.01	0.00	0.00	0.01	0.00	
Mg	1.70	2.02	1.22	1.44	1.74	2.07	1.85	1.97	1.25	1.45	1.58	
Total	4.53	4.68	4.65	4.72	5.01	5.26	4.71	4.77	5.26	4.76	4.74	
Ca	0.13	0.17	0.15	0.15	0.14	0.12	0.13	0.13	0.14	0.18	0.16	
Na	0.14	0.16	0.06	0.04	0.03	0.10	0.07	0.07	0.36	0.32	0.27	
K	0.38	0.31	0.19	0.17	0.11	0.29	0.17	0.22	0.29	0.28	0.26	
Total	0.65	0.64	0.40	0.35	0.28	0.51	0.38	0.42	0.78	0.78	0.69	

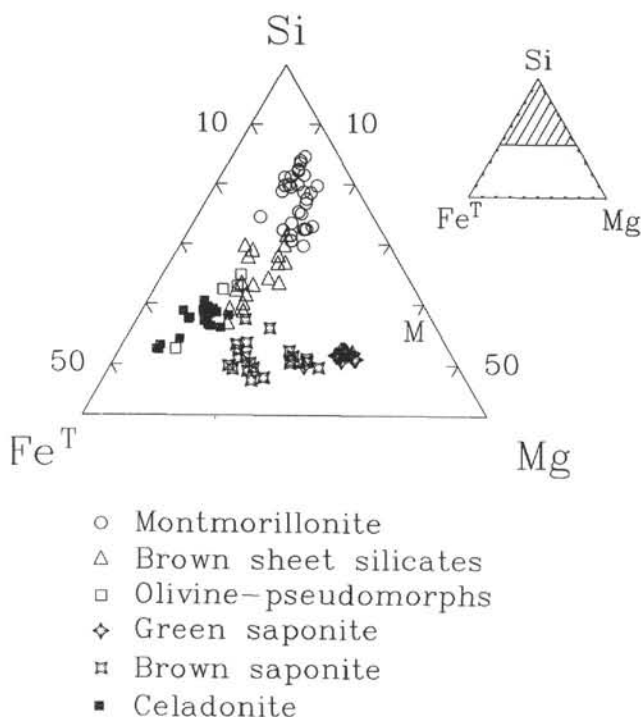


Figure 5. Compositional variation of sheet silicates from altered samples.

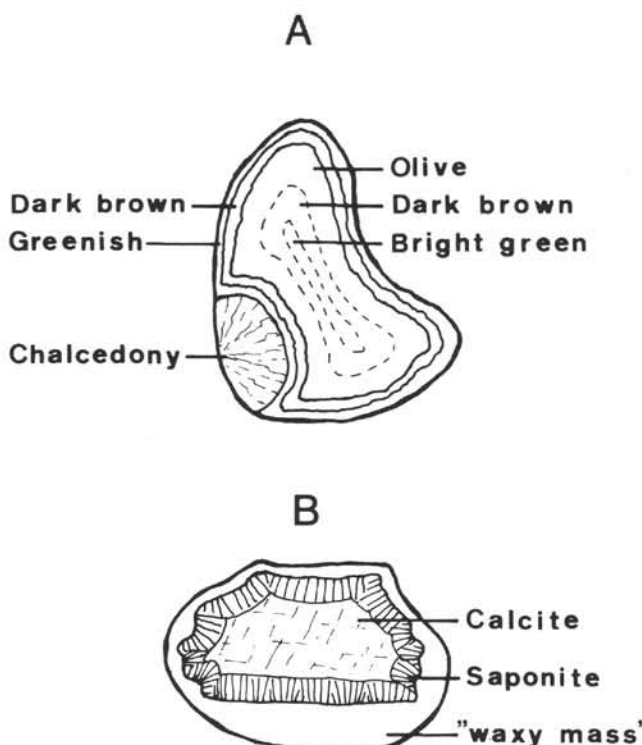


Figure 6. Sketch illustrating typical vesicle fillings. A. Vesicle filled by chalcedony and sheet minerals. Concentric layers of sheet minerals (greenish and dark brown) have sharp boundaries. The inner filling consists of varicolored sheet minerals grading from olive to dark brown to bright green, of which the latter is celadonite. B. Vesicle filled by "waxy mass" (showing geopetal texture in the lower part), radially arranged fibrous green saponite crystals, and blocky calcite.

#### Element Variation with $H_2O$ as an Alteration Index

Elements and element ratios plotted against  $H_2O$  as an index for alteration (Fig. 10) show positive correlations for Sr,  $CO_2$ , and  $Fe_2O_3/FeO$ , and negative correlations for CaO. Na<sub>2</sub>O and K<sub>2</sub>O also seem to increase with increasing  $H_2O$ . In comparison with the massive flow basalt samples, the clastic samples have distinctly higher FeO<sup>T</sup>,  $CO_2$ ,  $H_2O$ , and K<sub>2</sub>O concentrations, and higher K/Rb, K/Sr, and K/Ba ratios. In contrast, CaO, Sr, and V concentrations are lower (Fig. 10). The variations in these elements, and to a lower degree in Si, Ba, Y, Rb, and MgO do not systematically vary with depth, but with the degree of alteration, a measure of which is the increase in Fe<sub>2</sub>O<sub>3</sub>, K/Rb,  $CO_2$ , or  $H_2O$ .

#### Rare Earth Element Concentrations

The REE of the least altered basalts (Fig. 11, Table 7) display a significant enrichment of the LREE over the HREE ( $Ce_{cn}/Yb_{cn} = 3.2-4.1$ ), and have smooth and very similar chondrite normalized patterns without pronounced Eu-anomalies or flat HREE tails. Sample 119-738C-33R-1, 2-4 cm, from the top has a very slight positive Eu anomaly and the lowest REE concentrations. Sample 119-738C-33R-5, 22-25 cm, has the highest concentration in LREE and second lowest concentrations in HREE, while Sample 119-738C-36R-3, 37-40 cm, shows the second lowest LREE and higher HREE concentrations (Fig. 11).

## DISCUSSION

### Lithostratigraphy

The absence of glassy rinds, the large amount and size of vesicles (up to 25%), the high degree of oxidation, the lack of intercalated marine sediments (carbonate, fossils), and the formation as aa-flows indicate subaerial to shallow water eruption and emplacement of the basalt flows and the breccias from Unit VIII. The roundness of the clasts and the sedimentary matrix of Subunit VIIa are evidence for reworking in a shallow marine environment.

The basalt layers represent aa-lava flows. Thin lava layers within the breccias belong to lava clinkers associated with aa-flows. Breccias dominated by vesicular tachylitic clasts may represent top breccias whereas the basaltic clast dominated breccias may represent basal breccias. Thickness of the breccia units and angularity of the lithoclasts are interpreted to indicate provenance from a proximal fracture zone where small volume lava flows and larger volumes of breccia were generated.

### Alteration

In general, cold seawater alteration (e.g., Robinson et al., 1977; Donnelly et al., 1980; Lawrence, 1980; Staudigel and Hart, 1983; Bednarz and Schmincke, 1989) is characterized by a gain in  $H_2O$ , K<sub>2</sub>O, Ba, and Rb, a high oxidation, and a loss of CaO and minor Na<sub>2</sub>O, under temperatures lower than 40°C and not significantly different from the ocean bottom. Replacement of plagioclase by K-feldspar and formation of various sheet silicates and carbonate are the mineralogical expressions of the chemical changes.

Low-temperature alteration (e.g., Bednarz and Schmincke, 1989) is characterized by a small gain of K<sub>2</sub>O, a gain of Na<sub>2</sub>O, and MgO, and less depletion of CaO than during cold seawater alteration. Celadonite and saponite replace interstitial glass and fill voids, but both are also reported as a result of cold seawater alteration (Andrews, 1980). Plagioclase and clinopyroxene are fresh or altered to smectite and smectite/chlorite mixed minerals. Calcite is less abundant than in the cold seawater alteration zone. The secondary mineral assemblage indicates temperatures below 200°C.

Saponite and celadonite phases are typical mineral assemblages formed during cold seawater and low-temperature alteration at temperatures as low as 30°C (Seyfried et al., 1978; Andrews, 1979). Celadonite develops at oxidative conditions and a low pH from

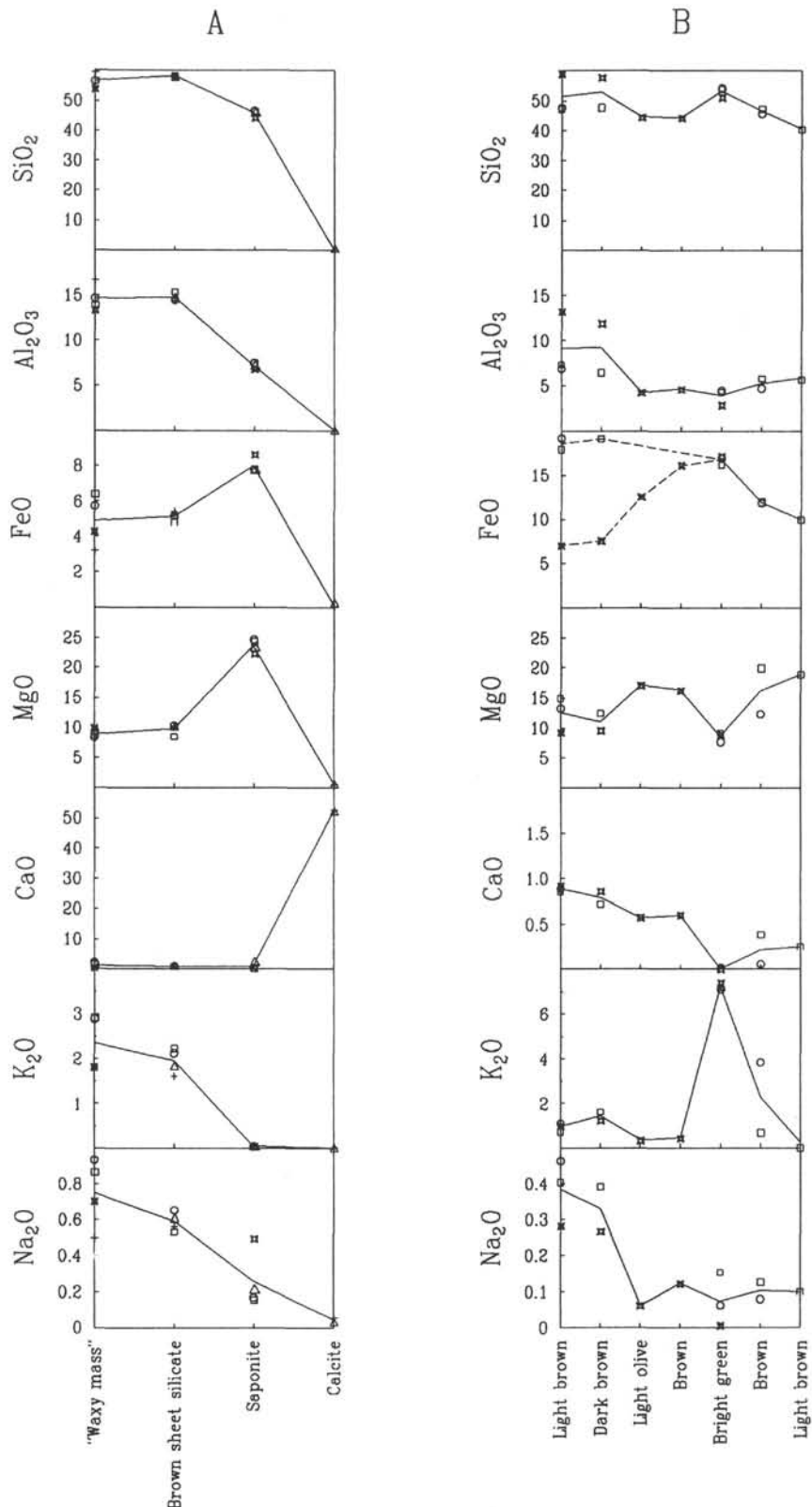


Figure 7. Variation of chemical composition of two distinct successions of secondary minerals in vesicles (left to right = rim to core; lack of symbol = mineral absent). Oxides in wt%. A. "Waxy mass"-light brown sheet silicate-green saponite-calcite. Four vesicles in Sample 119-738C-32R-5, 44–46 cm. B. Concentric layers of varicolored sheet minerals in Samples 119-738C-33R-3, 118–120 cm (circle and square), and 119-738C-36R-1, 148–150 cm (star).

**Table 4.** Major and trace element concentrations of basement samples and their ratios analyzed by XRF. VIIa = Unit VIIa, VIIb = Unit VIIb, b = basalt in Unit VIII, br = breccia in Unit VIII.

Original values												
Core, Section, Interval [cm]	32R-CC 0-4	32R-CC 12-14	33R-1 2-4	33R-1 129-132	33R-1 134-137	33R-2 59-62	33R-3 22-25	33R-3 38-41	33R-3 130-133	33R-4 68-71	33R-4 111-114	33R-5 22-25
Rock type	VIIa	VIIb	b	br	br	br	br	br	br	br	br	b
SiO <sub>2</sub>	44.50	44.40	50.70	47.60	49.96	49.10	49.30	49.30	50.90	49.70	47.43	51.04
TiO <sub>2</sub>	2.15	1.32	1.68	1.73	2.02	1.71	1.54	1.67	1.56	1.46	1.42	1.59
Al <sub>2</sub> O <sub>3</sub>	17.41	15.83	16.05	14.35	16.28	13.77	14.51	15.59	14.92	13.85	13.41	15.41
Fe <sub>2</sub> O <sub>3</sub>	15.25	8.98	6.13	11.00	9.04	9.42	8.88	8.00	7.54	8.69	8.42	5.27
FeO	1.16	1.36	4.17	1.87	2.89	2.63	2.40	3.04	3.27	2.94	3.02	4.64
MnO	0.14	0.08	0.16	0.11	0.09	0.14	0.11	0.14	0.14	0.16	0.17	0.20
MgO	1.44	2.06	5.49	4.39	4.00	5.27	5.54	5.14	5.40	5.34	5.33	5.62
CaO	7.67	11.69	9.35	7.79	6.83	7.43	7.71	8.78	6.78	7.59	10.21	9.10
Na <sub>2</sub> O	3.10	1.83	2.82	2.62	3.30	2.70	2.64	2.69	2.72	2.59	2.75	3.02
K <sub>2</sub> O	1.27	1.56	0.97	1.68	1.78	1.48	1.21	1.39	2.41	2.44	2.08	1.81
P <sub>2</sub> O <sub>5</sub>	0.49	0.14	0.19	0.28	0.23	0.25	0.16	0.18	0.19	0.18	0.18	0.21
Cr	142	85	219	163	229	48	119	130	97	87	88	100
Co	33	31	46	51	42	39	40	47	45	47	40	42
Ba	322	217	197	301	271	203	169	204	310	269	264	303
V	307	104	292	211	307	237	236	292	268	243	255	286
Ni	78	41	36	59	35	35	34	38	33	38	35	42
Cu	26	31	35	71	69	43	28	31	27	40	57	23
Zn	259	99	118	98	116	108	99	130	99	95	101	99
Rb	21	23	15	13	26	20	14	15	40	45	35	30
Sr	362	293	310	287	322	304	303	307	271	257	253	269
Y	55	23	29	38	22	47	35	33	29	30	34	33
Zr	187	137	154	161	164	157	136	142	140	129	127	140
Nb	12	8	10	9	9	8	7	8	8	8	7	8
CO <sub>2</sub>	1.87	4.97	0.14	2.17	1.27	3.29	2.21	2.11	0.21	2.28	3.63	0.22
H <sub>2</sub> O	4.30	4.52	2.34	3.07	3.47	3.29	3.42	2.57	2.77	3.14	2.70	1.43
Sum	100.93	98.85	100.34	98.80	101.32	100.61	99.75	100.74	98.94	100.49	100.88	99.70
Fe <sub>2</sub> O <sub>3</sub> /Fe O	13.10	6.62	1.47	5.89	3.13	3.59	3.69	2.63	2.31	2.95	2.78	1.14
Zr/Nb	15.58	17.13	15.40	17.89	18.22	19.63	19.43	17.75	17.50	16.13	18.14	17.50
Ti/Zr	68.93	57.76	65.40	64.42	73.84	65.30	67.88	70.50	66.80	67.85	67.03	68.09
Zr/Y	3.40	5.96	5.31	4.24	7.45	3.34	3.89	4.30	4.83	4.30	3.74	4.24
Y/Nb	4.58	2.88	2.90	4.22	2.44	5.88	5.00	4.13	3.63	3.75	4.86	4.13
Ba/Nb	26.83	27.13	19.70	33.44	30.11	25.38	24.14	25.50	38.75	33.63	37.71	37.88
K/Ba	32.74	59.68	40.88	46.33	54.53	60.52	59.44	56.56	64.54	75.30	65.41	49.59
K/Sr	29.12	44.20	25.98	48.59	45.89	40.42	33.15	37.59	73.83	78.82	68.25	55.86
K/Rb	502.05	563.07	536.84	1072.82	568.34	614.32	717.50	769.28	500.17	450.13	493.35	500.86
Ti/V	41.98	76.09	34.49	49.15	39.45	43.26	39.12	34.29	34.90	36.02	33.38	33.33

CO <sub>2</sub> - and H <sub>2</sub> O-free normalized values												
Core, Section, Interval [cm]	32R-CC 0-4	32R-CC 12-14	33R-1 2-4	33R-1 129-132	33R-1 134-137	33R-2 59-62	33R-3 22-25	33R-3 38-41	33R-3 130-133	33R-4 68-71	33R-4 111-114	33R-5 22-25
Rock type	VIIa	VIIb	b	br	br	br	br	br	br	br	br	b
SiO <sub>2</sub>	46.96	49.69	51.81	50.88	51.73	52.22	52.38	51.32	53.04	52.28	50.16	52.05
TiO <sub>2</sub>	2.27	1.48	1.72	1.85	2.09	1.82	1.64	1.74	1.63	1.54	1.50	1.62
Al <sub>2</sub> O <sub>3</sub>	18.37	17.72	16.40	15.34	16.86	14.65	15.42	16.23	15.55	14.57	14.18	15.72
Fe <sub>2</sub> O <sub>3</sub>	16.09	10.05	6.27	11.75	9.36	10.02	9.43	8.33	7.86	9.14	8.90	5.38
FeO	1.23	1.52	4.26	1.99	2.99	2.79	2.55	3.17	3.41	3.10	3.20	4.73
MnO	0.15	0.09	0.16	0.12	0.09	0.15	0.12	0.15	0.15	0.17	0.18	0.20
MgO	1.52	2.31	5.61	4.69	4.14	5.61	5.89	5.35	5.63	5.62	5.64	5.73
CaO	8.09	13.08	9.55	8.33	7.07	7.90	8.19	9.14	7.07	7.98	10.80	9.28
Na <sub>2</sub> O	3.27	2.05	2.88	2.80	3.42	2.87	2.80	2.80	2.83	2.72	2.91	3.08
K <sub>2</sub> O	1.34	1.75	0.99	1.80	1.84	1.57	1.29	1.45	2.51	2.57	2.20	1.85
P <sub>2</sub> O <sub>5</sub>	0.52	0.16	0.19	0.30	0.24	0.27	0.17	0.19	0.20	0.19	0.19	0.21
Cr	150	95	224	174	237	51	126	135	101	92	93	102
Co	35	35	47	55	43	41	42	49	47	49	42	43
Ba	340	243	201	322	281	216	180	212	323	283	279	309
V	324	116	298	226	318	252	251	304	279	256	270	292
Ni	82	46	37	63	36	37	36	40	34	40	37	43
Cu	27	35	36	76	71	46	30	32	28	42	60	23
Zn	273	111	121	105	120	115	105	135	103	100	107	101
Rb	22	26	15	14	27	21	15	16	42	47	37	31
Sr	382	328	317	307	333	323	322	320	282	270	268	274
Y	58	26	30	41	23	50	37	34	30	32	36	34
Zr	197	153	157	172	170	167	144	148	146	136	134	143
Nb	13	9	10	10	9	9	7	8	8	8	7	8
Normalization factor	1.06	1.12	1.02	1.07	1.04	1.06	1.06	1.04	1.04	1.05	1.06	1.02

Table 4. (continued).

Original values												
Core, Section, Interval [cm]	33R-5 109–112	34R-1 41–44	34R-2 108–111	34R-3 66–69	34R-4 39–42	34R-4 65–68	34R-5 32–35	34R-6 22–25	34R-6 61–64	34R-6 93–96	35R-1 88–91	35R-2 144–147
Rock type	b	br	b	b	b	br	br	b	br	b	b	b
SiO <sub>2</sub>	49.80	51.20	52.00	42.90	50.60	45.90	46.70	50.00	44.90	46.20	50.20	49.80
TiO <sub>2</sub>	1.69	1.51	1.56	1.29	1.62	1.44	1.52	1.71	1.43	1.63	1.63	1.68
Al <sub>2</sub> O <sub>3</sub>	15.39	13.87	14.53	12.16	14.68	13.23	14.04	15.63	13.17	14.35	15.17	15.34
Fe <sub>2</sub> O <sub>3</sub>	8.01	8.27	3.98	7.30	6.77	10.76	11.31	5.48	11.09	6.57	6.32	7.90
FeO	2.60	3.52	6.71	3.56	4.16	0.95	0.84	3.86	0.58	2.93	4.15	2.86
MnO	0.12	0.11	0.20	0.13	0.17	0.16	0.18	0.21	0.18	0.20	0.13	0.11
MgO	6.62	5.67	6.09	4.97	6.20	5.26	5.64	7.09	4.73	6.30	6.44	6.59
CaO	7.82	6.43	9.47	14.48	8.79	11.71	9.50	8.64	10.47	9.86	9.07	7.92
Na <sub>2</sub> O	2.82	2.63	2.58	2.66	2.64	2.53	2.49	2.83	1.93	2.60	2.64	2.81
K <sub>2</sub> O	0.69	2.42	1.08	1.39	1.38	1.75	1.21	0.71	3.38	1.03	0.52	0.65
P <sub>2</sub> O <sub>5</sub>	0.17	0.22	0.19	0.18	0.19	0.16	0.13	0.21	0.17	0.19	0.16	0.14
Cr	99	80	104	75	97	89	73	92	72	84	94	93
Co	44	36	41	36	43	39	41	57	33	45	51	44
Ba	209	270	317	267	316	270	132	290	406	176	194	215
V	303	243	271	247	277	190	162	309	149	274	290	309
Ni	29	28	27	32	31	27	39	30	26	35	31	27
Cu	29	66	32	76	74	163	63	85	38	144	100	31
Zn	92	97	101	99	98	84	122	117	83	104	103	96
Rb	11	41	27	20	23	9	5	9	11	11	5	11
Sr	323	248	264	251	286	250	282	315	222	300	308	321
Y	34	31	36	36	32	44	33	30	37	32	33	31
Zr	148	131	141	120	145	120	131	152	127	134	143	148
Nb	9	6	9	10	9	1	6	8	7	9	8	9
CO <sub>2</sub>	0.94	1.53	0.07	6.62	0.47	4.22	3.50	1.06	4.75	3.67	0.21	0.67
H <sub>2</sub> O	2.89	2.82	0.75	2.27	1.97	2.12	3.26	2.65	2.05	2.91	2.28	2.95
Sum	99.69	100.33	99.34	100.04	99.78	100.32	100.44	100.23	98.95	98.57	99.05	99.55
Fe <sub>2</sub> O <sub>3</sub> /FeO	3.08	2.35	0.59	2.05	1.63	11.35	13.45	1.42	19.27	2.24	1.52	2.76
Zr/Nb	16.44	21.83	15.67	12.00	16.11	120.00	21.83	19.00	18.14	14.89	17.88	16.44
Ti/Zr	68.46	69.10	66.33	64.45	66.98	71.94	69.56	67.44	67.50	72.92	68.33	68.05
Zr/Y	4.35	4.23	3.92	3.33	4.53	2.73	3.97	5.07	3.43	4.19	4.33	4.77
Y/Nb	3.78	5.17	4.00	3.60	3.56	44.00	5.50	3.75	5.29	3.56	4.13	3.44
Ba/Nb	23.22	45.00	35.22	26.70	35.11	270.00	22.00	36.25	58.00	19.56	24.25	23.89
K/Ba	27.41	74.41	28.28	43.22	36.25	53.81	76.10	20.32	69.11	48.58	22.25	25.10
K/Sr	17.73	81.01	33.96	45.97	40.06	58.11	35.62	18.71	126.39	28.50	14.02	16.81
K/Rb	520.74	490.00	332.06	576.96	498.10	1614.20	2008.99	654.90	2550.86	777.33	863.37	490.55
Ti/V	33.44	37.25	34.51	31.31	35.06	45.44	56.25	33.18	57.54	35.66	33.70	32.59
CO <sub>2</sub> - and H <sub>2</sub> O-free normalized values												
Core, Section, Interval [cm]	33R-5 109–112	34R-1 41–44	34R-2 108–111	34R-3 66–69	34R-4 39–42	34R-4 65–68	34R-5 32–35	34R-6 22–25	34R-6 61–64	34R-6 93–96	35R-1 88–91	35R-2 144–147
Rock type	b	br	b	b	b	br	br	b	br	b	b	b
SiO <sub>2</sub>	51.95	53.34	52.78	47.07	51.98	48.84	49.85	51.80	48.73	50.22	51.99	51.91
TiO <sub>2</sub>	1.76	1.57	1.58	1.42	1.66	1.53	1.62	1.77	1.55	1.77	1.69	1.75
Al <sub>2</sub> O <sub>3</sub>	16.05	14.45	14.75	13.34	15.08	14.08	14.99	16.19	14.29	15.60	15.71	15.99
Fe <sub>2</sub> O <sub>3</sub>	8.35	8.62	4.04	8.01	6.95	11.45	12.08	5.68	12.04	7.14	6.54	8.23
FeO	2.71	3.67	6.81	3.91	4.27	1.01	0.90	4.00	0.62	3.18	4.30	2.98
MnO	0.13	0.11	0.20	0.14	0.17	0.17	0.19	0.22	0.20	0.22	0.13	0.11
MgO	6.91	5.91	6.18	5.45	6.37	5.60	6.02	7.35	5.13	6.85	6.67	6.87
CaO	8.16	6.70	9.61	15.89	9.03	12.46	10.14	8.95	11.36	10.72	9.39	8.26
Na <sub>2</sub> O	2.94	2.74	2.62	2.92	2.71	2.69	2.66	2.93	2.09	2.83	2.73	2.93
K <sub>2</sub> O	0.72	2.52	1.10	1.52	1.42	1.86	1.29	0.74	3.67	1.12	0.54	0.68
P <sub>2</sub> O <sub>5</sub>	0.18	0.23	0.19	0.20	0.20	0.17	0.14	0.22	0.18	0.21	0.17	0.15
Cr	103	83	106	82	100	95	78	95	78	91	97	97
Co	46	38	42	39	44	42	44	59	36	49	53	46
Ba	218	281	322	293	325	287	141	300	441	191	201	224
V	316	253	275	271	285	202	173	320	162	298	300	322
Ni	30	29	27	35	32	29	42	31	28	38	32	28
Cu	30	69	32	83	76	173	67	88	41	157	104	32
Zn	96	101	103	109	101	89	130	121	90	113	107	100
Rb	11	43	27	22	24	10	5	9	12	12	5	11
Sr	337	258	268	275	294	266	301	326	241	326	319	335
Y	35	32	37	39	33	47	35	31	40	35	34	32
Zr	154	136	143	132	149	128	140	157	138	146	148	154
Nb	9	6	9	11	9	1	6	8	8	10	8	9
Normalization factor	1.04	1.04	1.02	1.10	1.03	1.06	1.07	1.04	1.09	1.04	1.04	1.04

Table 4. (continued).

Original values											
Core, Section, Interval [cm]	35R-3 15–18	35R-3 61–64	35R-3 71–73	35R-4 9–12	35R-4 61–64	35R-4 139–142	35R-6 6–9	36R-1 89–92	36R-2 143–146	36R-3 37–40	36R-3 98–101
Rock type	br	br	b	br	br	br	b	br	b	b	b
SiO <sub>2</sub>	47.00	48.50	48.20	48.40	47.70	46.00	48.90	50.10	51.50	50.80	51.10
TiO <sub>2</sub>	1.51	1.65	1.55	1.57	1.53	1.57	1.62	1.61	1.59	1.56	1.56
Al <sub>2</sub> O <sub>3</sub>	13.92	15.92	13.94	14.39	14.07	14.47	14.37	14.33	14.36	14.34	14.22
Fe <sub>2</sub> O <sub>3</sub>	10.68	9.67	7.78	9.29	8.12	10.71	6.13	6.67	3.47	3.73	3.84
FeO	2.09	1.99	3.79	3.12	2.03	1.77	4.48	4.43	7.78	7.40	7.68
MnO	0.13	0.14	0.15	0.14	0.16	0.12	0.20	0.17	0.27	0.26	0.26
MgO	6.31	5.17	5.15	5.89	5.64	4.65	6.15	6.23	6.45	6.53	6.41
CaO	8.37	7.06	9.88	8.62	9.55	10.17	9.69	9.02	9.78	9.73	9.71
Na <sub>2</sub> O	2.24	2.47	2.55	2.49	2.67	2.57	2.54	2.56	2.50	2.48	2.43
K <sub>2</sub> O	1.62	1.84	2.12	1.21	1.12	1.29	0.76	0.81	0.40	0.37	0.43
P <sub>2</sub> O <sub>5</sub>	0.11	0.17	0.18	0.19	0.23	0.17	0.20	0.18	0.19	0.18	0.19
Cr	84	93	98	86	78	85	86	85	87	95	
Co	43	39	41	42	34	34	38	37	43	42	39
Ba	112	221	300	139	220	221	213	498	287	276	281
V	231	267	276	250	208	205	276	276	272	272	262
Ni	43	30	30	34	22	30	27	27	31	32	29
Cu	50	70	35	55	49	46	51	39	42	49	56
Zn	84	94	103	98	111	96	103	91	110	111	92
Rb	8	10	33	8	10	7	14	15	6	5	9
Sr	259	288	254	281	306	281	302	304	287	283	281
Y	23	32	33	39	39	34	37	33	34	34	33
Zr	127	142	138	136	139	135	142	143	139	135	136
Nb	8	8	6	7	5	6	8	9	8	8	9
CO <sub>2</sub>	4.08	1.90	1.94	1.76	4.39	3.85	1.24	0.28	0.06	0.12	0.08
H <sub>2</sub> O	3.57	3.27	2.22	3.13	3.40	2.69	2.42	2.57	1.17	1.32	1.26
Sum	101.74	99.89	99.58	100.32	100.72	100.15	98.83	99.11	99.66	98.96	99.29
Fe <sub>2</sub> O <sub>3</sub> /FeO	5.12	4.85	2.05	2.97	4.01	6.05	1.37	1.50	0.45	0.50	0.50
Zr/Nb	15.88	17.75	23.00	19.43	27.80	22.50	17.75	15.89	17.38	16.88	15.11
Ti/Zr	71.28	69.66	67.34	69.21	65.99	69.72	68.39	67.50	68.58	69.28	68.77
Zr/Y	5.52	4.44	4.18	3.49	3.56	3.97	3.84	4.33	4.09	3.97	4.12
Y/Nb	2.88	4.00	5.50	5.57	7.80	5.67	4.63	3.67	4.25	4.25	3.67
Ba/Nb	14.00	27.63	50.00	19.86	44.00	36.83	26.63	55.33	35.88	34.50	31.22
K/Ba	120.08	69.12	58.66	72.27	42.26	48.46	29.62	13.50	11.57	11.13	12.70
K/Sr	51.93	53.04	69.29	35.75	30.38	38.11	20.89	22.12	11.57	10.85	12.70
K/Rb	1681.07	1527.49	533.31	1255.62	929.78	1529.87	450.66	448.29	553.44	614.32	396.63
Ti/V	39.19	37.05	33.67	37.65	44.10	45.91	35.19	34.97	35.04	34.38	35.70
CO <sub>2</sub> - and H <sub>2</sub> O-free normalized values											
Core, Section	35R-3 15–18	35R-3 61–64	35R-3 71–73	35R-4 9–12	35R-4 61–64	35R-4 139–142	35R-6 6–9	36R-1 89–92	36R-2 143–146	36R-3 37–40	36R-3 98–101
Rock type	br	br	b	br	br	br	b	br	b	b	b
SiO <sub>2</sub>	49.95	51.20	50.51	50.72	51.33	49.14	51.38	52.05	52.32	52.09	52.17
TiO <sub>2</sub>	1.60	1.74	1.62	1.65	1.65	1.68	1.70	1.67	1.62	1.60	1.59
Al <sub>2</sub> O <sub>3</sub>	14.80	16.81	14.61	15.08	15.14	15.46	15.10	14.89	14.59	14.70	14.52
Fe <sub>2</sub> O <sub>3</sub>	11.35	10.21	8.15	9.73	8.74	11.44	6.44	6.93	3.53	3.83	3.92
FeO	2.22	2.11	3.97	3.27	2.18	1.89	4.71	4.60	7.90	7.59	7.84
MnO	0.14	0.15	0.16	0.15	0.17	0.13	0.21	0.18	0.27	0.27	0.27
MgO	6.71	5.46	5.40	6.17	6.07	4.97	6.46	6.47	6.55	6.70	6.54
CaO	8.90	7.45	10.35	9.03	10.28	10.86	10.18	9.37	9.94	9.98	9.91
Na <sub>2</sub> O	2.38	2.61	2.67	2.61	2.87	2.75	2.67	2.66	2.54	2.54	2.48
K <sub>2</sub> O	1.72	1.94	2.22	1.27	1.21	1.38	0.80	0.84	0.41	0.38	0.44
P <sub>2</sub> O <sub>5</sub>	0.12	0.18	0.19	0.20	0.25	0.18	0.21	0.19	0.19	0.18	0.19
Cr	89	98	103	90	84	91	90	88	85	89	97
Co	46	41	43	44	37	36	40	38	44	43	40
Ba	119	233	314	146	237	236	224	517	292	283	287
V	246	282	289	262	224	219	290	287	276	279	267
Ni	46	32	31	36	24	32	28	28	31	33	30
Cu	53	74	37	58	53	49	54	41	43	50	57
Zn	89	99	108	103	119	103	108	95	112	114	94
Rb	9	11	35	8	11	7	15	16	6	5	9
Sr	275	304	266	294	329	300	317	316	292	290	287
Y	24	34	35	41	42	36	39	34	35	35	34
Zr	135	150	145	143	150	144	149	149	141	138	139
Nb	9	8	6	7	5	6	8	9	8	8	9
Normalization factor	1.06	1.06	1.05	1.05	1.08	1.07	1.05	1.04	1.02	1.03	1.02

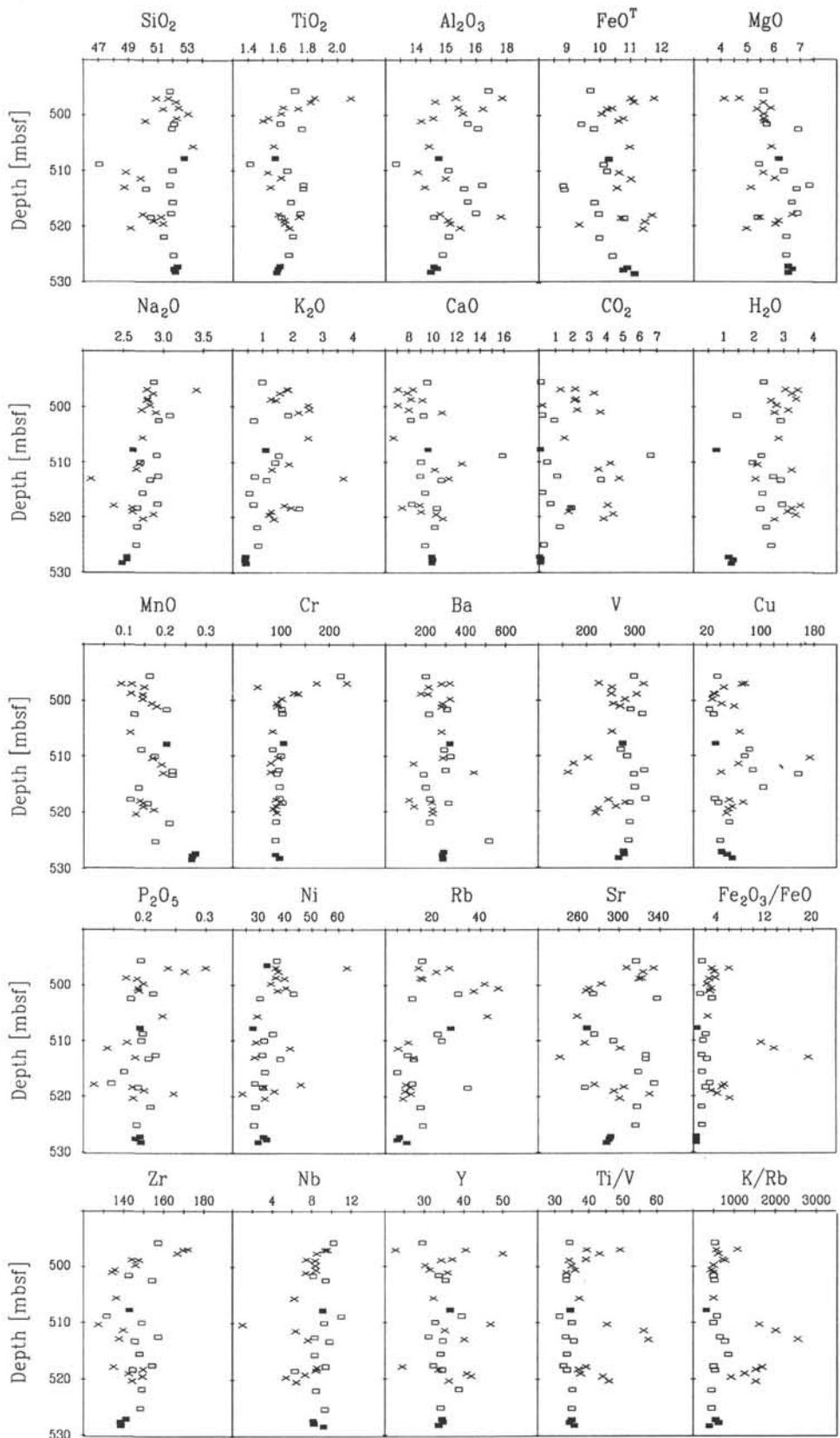


Figure 8. Variation of major and trace element concentrations and element ratios of Unit VIII samples. Oxides in wt%, elements in ppm. Crosses represent breccias, quadrangles represent basalts, and filled quadrangles represent the four freshest basalts.

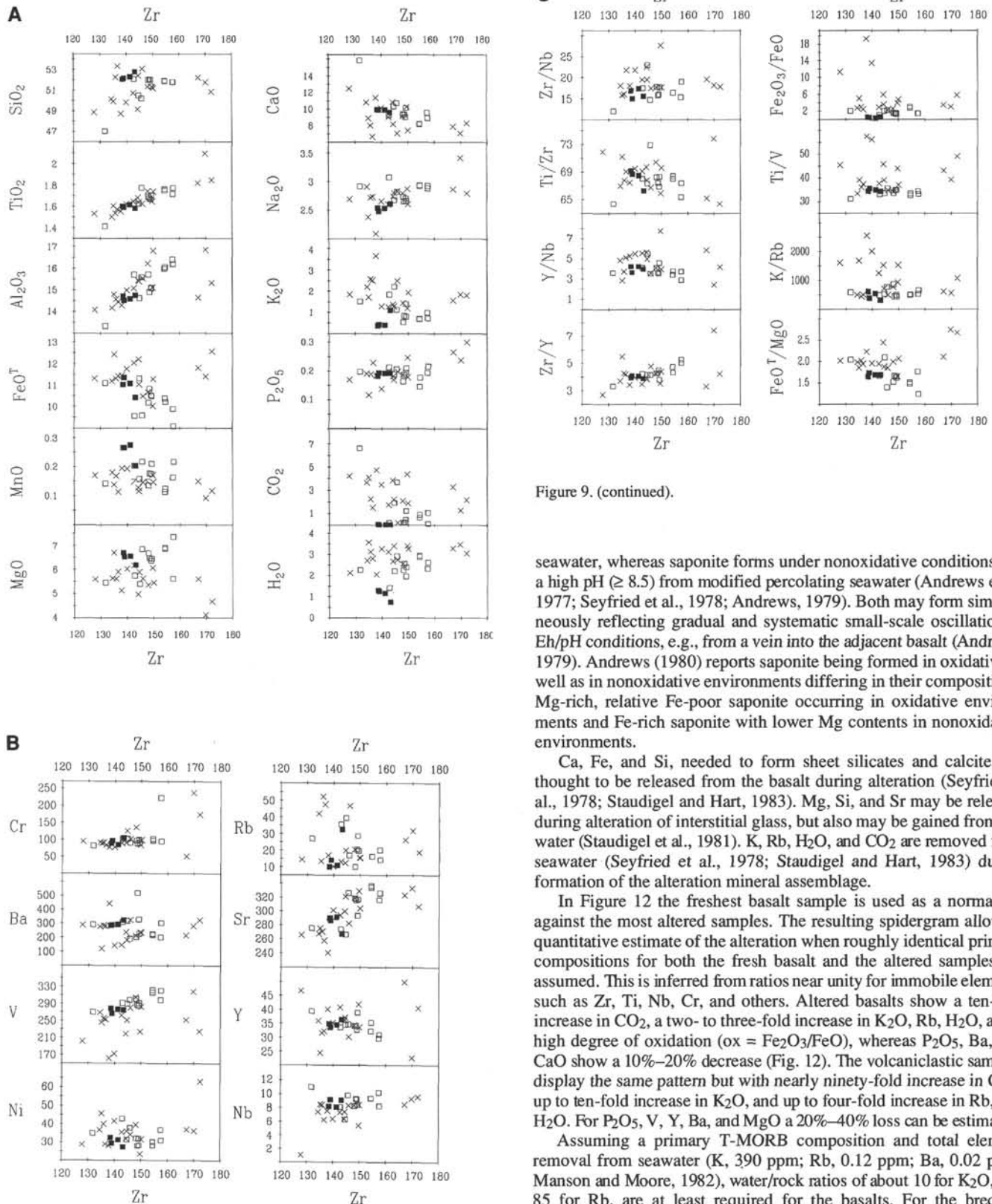


Figure 9. (continued).

seawater, whereas saponite forms under nonoxidative conditions and a high pH ( $\geq 8.5$ ) from modified percolating seawater (Andrews et al., 1977; Seyfried et al., 1978; Andrews, 1979). Both may form simultaneously reflecting gradual and systematic small-scale oscillation of Eh/pH conditions, e.g., from a vein into the adjacent basalt (Andrews, 1979). Andrews (1980) reports saponite being formed in oxidative as well as in nonoxidative environments differing in their compositions: Mg-rich, relative Fe-poor saponite occurring in oxidative environments and Fe-rich saponite with lower Mg contents in nonoxidative environments.

Ca, Fe, and Si, needed to form sheet silicates and calcite, are thought to be released from the basalt during alteration (Seyfried et al., 1978; Staudigel and Hart, 1983). Mg, Si, and Sr may be released during alteration of interstitial glass, but also may be gained from sea water (Staudigel et al., 1981). K, Rb, H<sub>2</sub>O, and CO<sub>2</sub> are removed from seawater (Seyfried et al., 1978; Staudigel and Hart, 1983) during formation of the alteration mineral assemblage.

In Figure 12 the freshest basalt sample is used as a normalizer against the most altered samples. The resulting spidergram allows a quantitative estimate of the alteration when roughly identical primary compositions for both the fresh basalt and the altered samples are assumed. This is inferred from ratios near unity for immobile elements such as Zr, Ti, Nb, Cr, and others. Altered basalts show a ten-fold increase in CO<sub>2</sub>, a two- to three-fold increase in K<sub>2</sub>O, Rb, H<sub>2</sub>O, and a high degree of oxidation (ox = Fe<sub>2</sub>O<sub>3</sub>/FeO), whereas P<sub>2</sub>O<sub>5</sub>, Ba, and CaO show a 10%–20% decrease (Fig. 12). The volcaniclastic samples display the same pattern but with nearly ninety-fold increase in CO<sub>2</sub>, up to ten-fold increase in K<sub>2</sub>O, and up to four-fold increase in Rb, and H<sub>2</sub>O. For P<sub>2</sub>O<sub>5</sub>, V, Y, Ba, and MgO a 20%–40% loss can be estimated.

Assuming a primary T-MORB composition and total element removal from seawater (K, 390 ppm; Rb, 0.12 ppm; Ba, 0.02 ppm; Manson and Moore, 1982), water/rock ratios of about 10 for K<sub>2</sub>O, and 85 for Rb, are at least required for the basalts. For the breccias water/rock ratios of 30 and 185 are required for K<sub>2</sub>O and Rb, respectively. The contribution of seawater Ba to the enriched Ba concentrations is negligible if reasonable water/rock ratios are considered. Ba may therefore be either derived from upwelling hydrothermal solutions (Mottl and Holland, 1978; Seyfried and Bischoff, 1979), for

Figure 9. A. Variation of major elements of Unit VIII samples vs. Zr. Oxides in wt%. B. Variation of trace elements of Unit VIII samples vs. Zr. Elements in ppm. C. Variation of element ratios of Unit VIII samples vs. Zr. Symbols as in Figure 8.

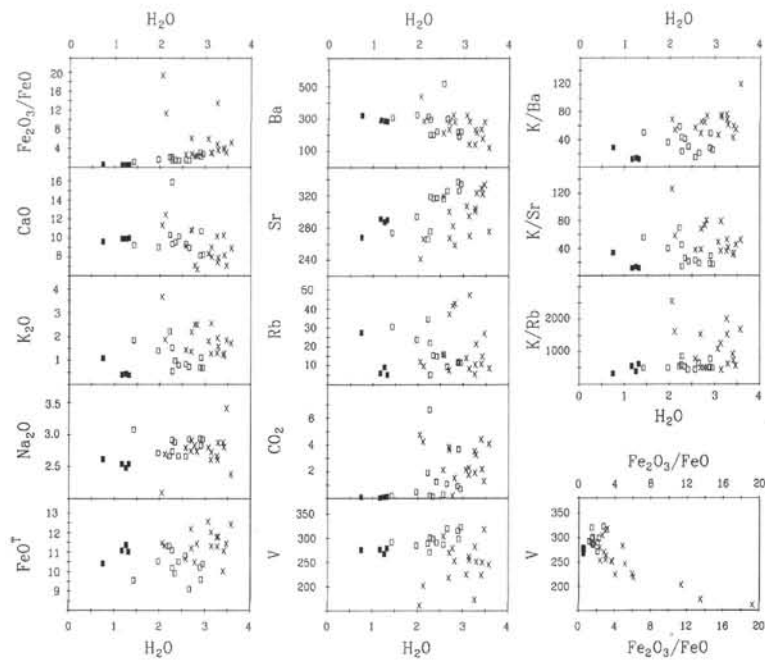


Figure 10. Variation of mobile elements and element ratios of Unit VIII samples vs.  $H_2O$  and  $V$  vs.  $Fe_2O_3/FeO$ . Oxides in wt%, elements in ppm. Symbols as in Figure 8.

**Table 5. CIPW norms of the freshest samples. Assumed  $Fe_2O_3 = 2\%$ .**

	119-738-34R-2 108-111 cm	119-738-36R-2 143-146 cm	119-738-36R-3 37-40 cm	119-738-36R-3 98-101 cm
Quartz	3.31	4.05	3.68	3.95
Orthoclase	6.50	2.42	2.25	2.60
Albite	22.25	21.58	21.58	21.07
Anorthite	25.30	27.24	27.63	27.23
Diopside	17.10	16.89	16.46	16.73
Hypersthene	18.97	21.22	21.70	21.80
Magnetite	2.96	2.96	2.97	2.97
Ilmenite	3.02	3.08	3.04	3.04
Apatite	0.44	0.44	0.42	0.44
Calcite	0.16	0.14	0.27	0.18

which there is no indication in our basalts, or be a primary feature of the basalt magma, which is assumed here.  $V$  is leached and removed from the breccias (Ti-magnetite therein) probably because of higher water/rock ratios (Table 8.)

The significantly higher alteration of breccias compared to lava flows is attributed to higher water/rock ratios as previously discussed due to higher permeabilities of the breccias (porosities are about 35%; Barron, Larsen, et al., 1989) and has previously been reported, e.g., from Icelandic basalts (Mehegan and Robinson, 1982; Viereck et al., 1982).

The chemical and mineralogical changes of the basement rocks are mainly due to low-temperature alteration. The gains of  $K_2O$ ,  $Rb$ , and  $H_2O$ , and the loss of  $CaO$  as well as the alteration of plagioclase and clinopyroxene to sheet silicates indicate low-temperature alteration. The occurrence of celadonite and saponite limits the alteration temperature to about 170°C (Seyfried et al., 1978; Seyfried and Bischoff, 1979; Andrews, 1979, 1980). This is in agreement with the whole secondary mineral assemblage (Fig. 13) and the lack of secondary high-temperature phases such as sphene, chlorite, or specific zeolite.

The occurrence of Fe-oxides and Fe-hydroxides, celadonite, and green and brown saponite clearly reflects changing Eh/pH conditions during alteration.

The high oxidation and abundant calcite may be due to subsequent final cold seawater alteration. Cold seawater alteration may not have

**Table 6. Incompatible trace element ratios of Mesozoic N/T/P-MORB, OIB, and CFB from the Southern Hemisphere.**

	1	2	3	4	5	6	7	8	9	10	11	12	13	14	15
Zr/Nb	14–19	>17	8–12	6–7	<6	7–9	11–13	15–31	13–31	18–28	5–11	25	30	20.8	16.7
Zr/Y	3.3–5.3	1.8–3.6	3.6–6.2	6.1–7.9	>14	3.6–4.7	6.6–9.9	2.5–5.5	2.9–5.3	2.5–4.4	3.2–5.2	2.5	2.3	3.9	5.4
Y/Nb	2.9–5.5	>8	1.3–3.0	0.9–1.2	<0.3	1.5–2.6	1.2–1.9	1.7–12.3	2.5–10	3–9.3	1.3–4.7	10.2	12.7	4.9	3.1
Ba/Nb	34–39	5–17	6–13	6–10	9–15	10–16	11–18	31–44	8–28	<7	3.3	4.6	36	35	

1 = T-MORB from ODP Leg 119, Site 738; 2 = N-MORB from SWIR (LeRoex et al., 1983); 3 = T-MORB from SWIR (LeRoex et al., 1983); 4 = E/P-MORB from SWIR (LeRoex et al., 1983); 5 = OIB from ODP Leg 120, Site 748 (Bitschene et al., in prep); 6 = tholeiite from Kerguelen Island (Storey et al., 1988); 7 = Na-alkali basalt from Kerguelen Island (Storey et al., 1988); 8 = tholeites from SEIR (Dosso et al., 1988); 9 = low-Ti CFB from the Paraná Basin/South America (Bitschene, 1987; Mantovani et al., 1988); 10 = CFB from Rajmahal Trap/India (Mahoney et al., 1983); 11 = MORB from NER (Mahoney et al., 1983); 12 = N2-MORB (Viereck et al., 1989); 13 = N1-MORB (Viereck et al., 1989); 14 = Central Karoo low-Mg CFB from Lesotho (Erlank, 1984); 15 = CFB from the Etendeka-Formation/Namibia (Duncan et al., 1984).

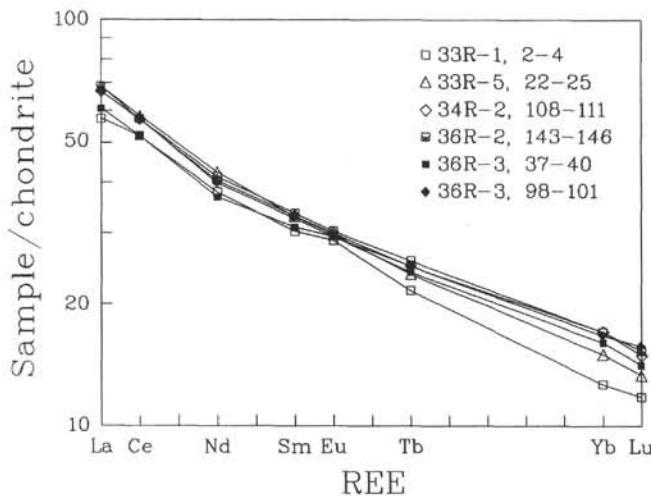


Figure 11. Variation of chondrite-normalized REE concentrations of selected Hole 738C samples. Normalization values from Sun and McDonough (1989).

been very effective as the typical replacement of groundmass-plagioclase by K-feldspar, and the resulting chemical changes were not observed. It may have been terminated by early sealing of the channelways.

### PETROGENESIS

The incompatible and immobile trace elements Zr, Nb, Y, Ta, and Ti, and the REE and their ratios are considered to represent original magma and source characteristics not affected by secondary alteration processes. These elements are used for characterization of the basaltic magmas and explanation of differences within the complete suite of basalts and breccias. Rb, K, Ba, and Th have to be treated separately,

Table 7. REE and trace element concentrations analyzed by INAA of selected Hole 738C samples. Na and Fe in wt%, other elements in ppm. cn = chondrite normalized.

Section, Interval	33R-1 2-4	33R-5 22-25	34R-2 108-111	36R-2 143-146	36R-3 37-40	36R-3 98-101
Na	2.19	2.22	2.16	2.06	2.03	2.04
Sc	36.1	36.7	35.2	35.2	35.1	35.0
Cr	229	104	96	84	87	84
Fe	7.45	7.35	8.12	8.59	8.50	8.87
Co	50.0	45.3	45.5	45.9	46.5	43.6
Rb	23	38	22	<8	<8	<11
Sr	360	292	269	321	299	262
Ba	164	352	280	266	252	229
La	13.6	16.3	15.8	16.3	14.4	15.8
Ce	31.9	35.7	35.0	35.1	31.9	35.2
Nd	17.7	19.8	18.9	19.3	17.2	18.6
Sm	4.64	5.05	5.06	5.14	4.75	5.00
Eu	1.67	1.73	1.74	1.76	1.71	1.71
Tb	.81	.89	.93	.96	.90	.93
Yb	2.16	2.56	2.91	2.91	2.74	2.85
Lu	.30	.34	.38	.39	.36	.40
Hf	4.1	3.6	3.6	3.7	3.6	3.5
Ta	.64	.55	.54	.55	.55	.53
Th	2.7	2.1	2.2	2.2	2.2	2.2
U	<.15	.37	.22	.20	<.15	<.15
(Ce/Yb)cn	4.10	3.87	3.34	3.35	3.23	3.43

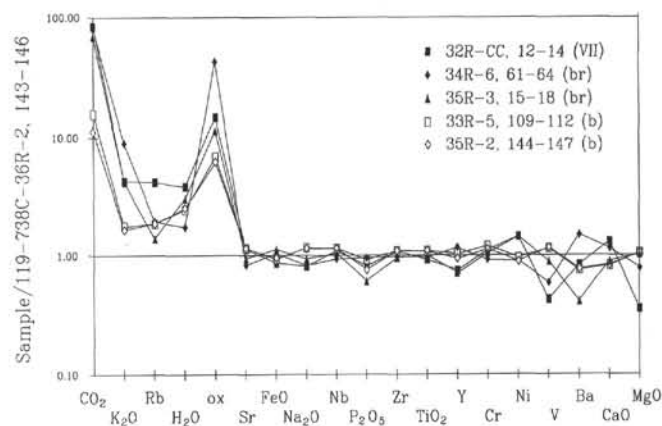


Figure 12. Spidergram showing alteration of selected Hole 738C samples. Concentrations are normalized against the freshest sample. VII = Unit VII, b = basalt of Unit VIII, br = breccia of Unit VIII, ox =  $\text{Fe}_2\text{O}_3/\text{FeO}$ .

because alteration may lead to precipitation or mobilization of these elements. As shown in the alteration section, high Ba (and low Rb and  $\text{K}_2\text{O}$ ) concentrations of the least altered samples are primary features of the magma. These samples (see norms in Table 5) are used to constrain source regions and to make comparisons with other tholeiitic basalts.

### Magma Characteristics and Comparison with Other Mesozoic Southern Hemisphere Basalts

The freshest Site 738 basalts have Rb concentrations between 5 and 9 ppm, higher than Rb concentrations from the freshest N-MORB glasses (0.4–4 ppm; LeRoex, 1987) or N1-MORB (1.4 ppm) and N2-MORB (1.8 ppm; Viereck et al., 1989), but equivalent to average T-MORB from the southern oceans (5.9 ppm; LeRoex, 1987).  $\text{K}_2\text{O}$  concentrations are between 0.37% and 0.42%, which is less than average southern ocean T-MORB (0.56%; LeRoex, 1987), and more than N-MORB (<0.11%; LeRoex 1987; Viereck et al. 1989). Ba concentrations for average Southern Ocean T-MORB (90 ppm;

Table 8. Alteration of basement rocks at Hole 738C.

	1	2a/b	3	4	5
SiO <sub>2</sub>	52.40	0.997/1.011	52.26	52.98	-
MgO	6.50	0.995/0.889	6.47	5.78	-
FeOT	10.99	0.954/1.082	10.49	11.89	8.67
K <sub>2</sub> O	0.58	1.983/3.379	1.15	1.96	0.56
Na <sub>2</sub> O	2.55	1.133/1.114	2.89	2.84	-
CaOcorr	9.76	0.829/0.561	8.09	5.48	-
CO <sub>2</sub>	0.08	18.12/34.62	1.45	2.77	-
H <sub>2</sub> O	1.13	2.133/2.637	2.41	2.98	-
Rb	6.8*	2.579/2.981	17.54	20.27	5.9
Sr	284.45	1.107/1.073	314.80	305.19	286
Ba	296.12	0.953/0.870	282.10	257.74	90
ox	0.31	1.968/2.548	0.61	0.79	-
K/Rb	474.11	1.204/2.329	570.99	1104.34	788
K/Sr	17.27	1.814/3.191	31.33	55.11	16.2
K/Ba	15.92	2.174/4.094	34.62	65.19	51.7
Ti/V	34.91	0.970/1.196	33.88	41.76	44.6

1 = mean of four freshest basalts (Samples 119-738C-34R-2, 108-111 cm; -36R-2, 143-146 cm; -36R-3, 37-40 cm; -36R-3, 98-101 cm); 2 = alteration factor: (a) mean of basalts/mean of four freshest basalts and (b) mean of breccias/mean of four freshest basalts; 3 = mean of basalts except the four freshest basalts; 4 = mean of breccias; 5 = T-MORB (LeRoex 1987); \* = only three freshest basalts

119–738C–  
Core, Section,  
Interval [cm]

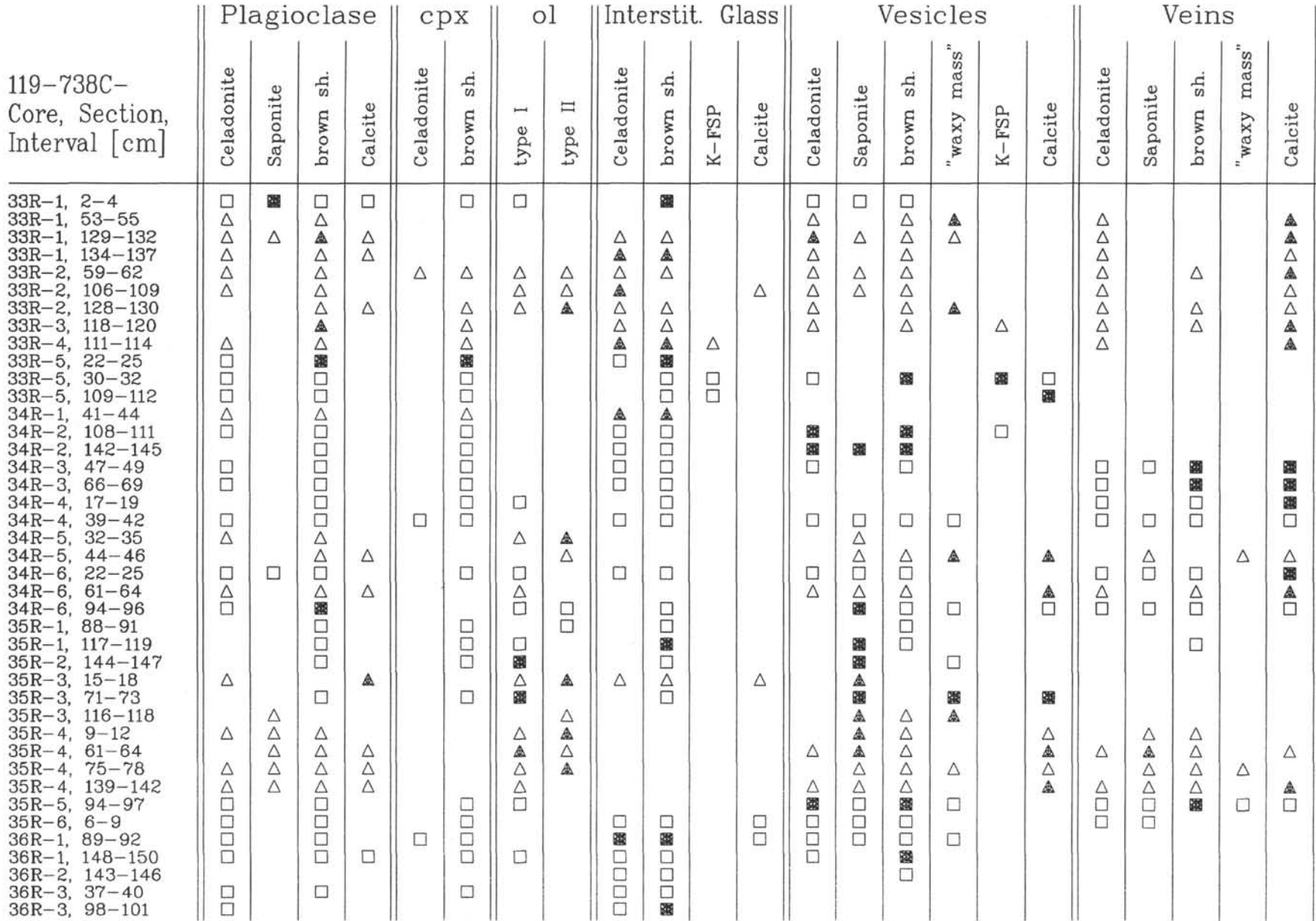


Figure 13. Stratigraphic distribution of secondary minerals and place of occurrence of Unit VIII samples. Squares = basalt, triangles = breccia, open symbols = minor, filled symbols = major, cpx = clinopyroxene, ol = olivine, interstit. glass = former interstitial glass.

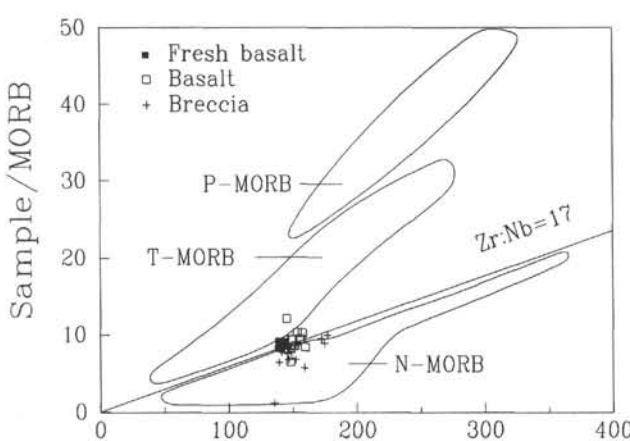


Figure 14. Variation of Nb vs. Zr. Reference fields for Southern Ocean MORB-types from LeRoex (1987).

LeRoex, 1987) and P-MORB (163 ppm; LeRoex, 1987) are significantly lower than in fresh Site 738 basalts ( $290 \pm 10$  ppm). The high Ba and Th concentrations are considered to be primary features, as well as the low Nb and Ta concentrations.

Tholeiitic MORB are customarily divided into LREE depleted N-MORB, and LREE enriched E-MORB (e.g., Sun et al., 1979; Viereck et al., 1989). Compared to N-MORB types (e.g., Klein and Langmuir, 1988; Viereck et al., 1989), the Site 738 basalts have distinctly higher LREE/HREE ratios ( $>3$  for Site 738 basalts;  $<1$  for N-MORB types) and higher HFSE concentrations, which confirms their enriched (E-MORB) character. E-MORB are furthermore divided into transitional basalts (T-MORB with relatively small LREE enrichments and Zr/Nb ratios between 10 and 17), and plume-type MORB (P-MORB with low Zr/Nb ratios between 4 and 7 and high LREE/HREE<sub>en</sub> ratios; e.g., LeRoex 1987). Ocean island basalts (OIB) have P-MORB trace element ratios and isotope characteristics.

LREE/HREE (3.2–4.1) and Zr/Nb (14–19, Fig. 14) ratios of Site 738 basalts are intermediate between N-MORB and P/T-MORB (Tables 7 and 9, and Figs. 14 and 15). The observed trace element characteristics (Fig. 15, Table 9) have a close match with T-MORB from the Southwest Indian Ridge, and even a better match with continental flood basalts. Ba concentrations and Ba/Nb ratios of Site 738 basalts are particularly useful in demonstrating the close relationship to Mesozoic continental flood basalts.

### Magma Evolution

Site 738 basalt flows have low Ni (32 +11/-5 ppm) and moderate Cr (95 +8/-13 ppm, except for the topmost sample) concentrations. The petrogenetic implications would be olivine, Cr-clinopyroxene and minor Cr-spinel fractionation leading to the evolved basaltic composition that is also indicated by  $\text{MgO} < 7.35\%$ . Fractionation of about 8% of olivine with Kd for Ni of about 15 would lower an initial Ni concentration of 250 ppm (primitive MORB) to the observed 30–40 ppm level. Cr-enrichment and respective clinopyroxene accumulation of the topmost samples may indicate the final eruption pulse, when clinopyroxene-enriched “leftovers” are tapped and erupted. Admixture of only 1%–2% of Cr- (and Mg-) rich clinopyroxene (Cr concentration about 10,000 ppm) to the basaltic magma is capable of raising average bulk-rock Cr concentrations from 95 ppm to the observed 240 ppm level. Such Cr- and Mg-rich clinopyroxene phenocrysts with up to 1.20%  $\text{Cr}_2\text{O}_3$  were found within the topmost sample.

Considering the whole data set, some variations in immobile element concentrations are observed, which do not comply with simple fractional crystallization:

1. The chemically more evolved samples ( $\text{Zr} > 150$  ppm) display the highest compatible element abundances ( $\text{Cr} > 95$  ppm;  $\text{MgO} > 6.5\%$ ), what is not compatible with fractional crystallization.

2.  $\text{Al}_2\text{O}_3$ ,  $\text{Na}_2\text{O}$ ,  $\text{Sr}$ ,  $\text{TiO}_2$ , and  $\text{V}$  are positively correlated with  $\text{Zr}$  and negatively correlated with  $\text{MgO}$  which indicates fractional crystallization of olivine and clinopyroxene without participation of Fe-Ti-oxide and major plagioclase fractionation; Ti and V increase and Fe decreases with increasing  $\text{Zr}$  (Figs. 9) precluding ilmenite or Ti-magnetite fractionation, and favoring early Fe incorporation into the pyroxenes or mixing of different magma batches.

To explain the observed trends in element variations two slightly different magma batches are inferred which underwent the same fractional crystallization process:

1. One (late?) batch has a more primitive and incompatible element enriched, more alkalic composition with high Al, Sr, Ti, V, Zr, and Mg, and low Fe concentrations.

2. Another batch has a more tholeiitic, evolved composition with significantly lower Al etc., and higher Fe concentrations.

The REE patterns (Fig. 11) support the idea of two slightly different magmas. Two different slopes and crossing of the lines indicate two different batches, one being more enriched in incompatible and LREE elements than the other. The wide range in plagioclase compositions, distinct for each subset, also supports the existence of compositionally slightly different magma batches. Olivine, clinopyroxene, and very minor plagioclase (no visible negative Eu anomaly) fractionation led to the evolved basalt compositions, which have also been found by LeRoex et al. (1983) in fracture zones of the Southwest Indian Ridge.

### Source Region

Normalization of the trace element budget of the three least altered basalts against N-MORB is used to further constrain possible source regions and contaminants (Fig. 16). The following information can be drawn from the trace element pattern (Fig. 16):

1. Ba and Th are strongly enriched with respect to the N-MORB normalizer.

2. The High-Field-Strength-Elements (HFSE) Ta, Nb, Zr, Hf, and Ti are only very slightly enriched, and a Ta and Nb trough is evident. Cr also seems to be depleted, although this may be caused by fractional crystallization.

3. The LREE, with Ce as indicator, are enriched; the HREE, with Yb as an indicator, are slightly depleted (compare Fig. 11).

4. Sr, Rb, and K are less enriched than the LREE, and especially Ba and Th. The slight enrichment in K and Rb against MORB may be due to fractionation processes. In other words, the low K and Rb concentrations bear N-MORB signature.

Significant upper crustal, granitic material to contaminate Site 738 can be excluded, as it should cause  $\text{SiO}_2$ , Sr, K, and Rb enrichment in the fresh samples. When enriched, this is due to alteration processes as previously discussed.

Site 738 basalts partially resemble plume-component-bearing basalts from Iceland (Rison and Craig, 1983), Hawaii (e.g., Frey and Clague, 1983) and some Columbia River basalts (Brandon and Goles, 1988). The similarities include the Ba, and partially the Th enrichment, the Sr, K, and Rb depletion, and the LREE enrichment. Smooth trace element patterns should be expected, if only a plume-derived, enriched component would be responsible for the enriched character of the three Site 738 basaltic samples. To thus explain the particular Ba, Th, and LREE enrichment, a complementary source has to be invoked that specifically contributes these elements and retains HFSE, especially Nb and Ta.

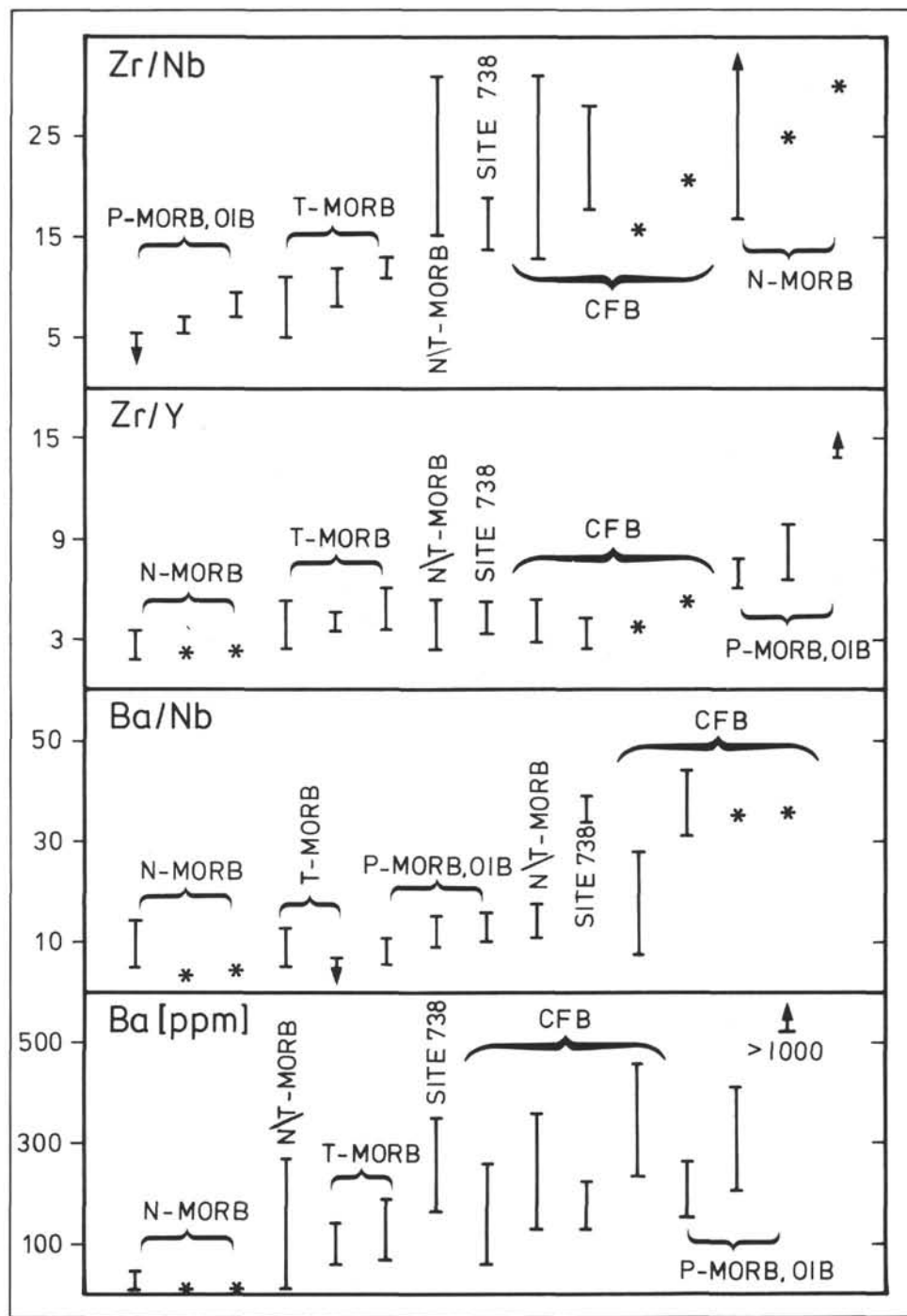


Figure 15. Zr/Nb, Zr/Y, Ba/Nb ratios, and Ba concentrations of various oceanic basalts and continental basalts from southern hemisphere divergent plate boundaries, compared with Site 738 T-MORB. For references see Table 9.

Low Ti/Zr ratios (64–73) and the high LREE/HREE ratios point to an enriched-mantle source, while the Zr/Y ratios (3.3–5.3) and relatively low Rb, K, and Sr abundances (Fig. 16) may point to a less-enriched to depleted source component. Finally, a third source component is inferred to be responsible for the Ba and Th hump, the Nb and Ta trough, the high Ba/Nb ratios, and the DUPAL isotope characteristics (Alibert, this volume).

High Ba/Ta (>300), Th/Ta (>4), and low Ta/La (<0.03) ratios are considered as evidence for contamination of continental flood basalts with some sort of crustal material (Loubet et al., 1988). Site 738 basalts

have Ba/Ta ratios around 480, a Th/Ta ratio of 4, and a Ta/La ratio of 0.034, which strongly point to crustal involvement. Further evidence for crustal derived contamination comes from the Nb and Ta troughs (Fig. 16), the small though recognizable P, Zr, Hf, Ti, and Yb depletion, and the Ba and Th bows, as emphasized by Thompson et al. (1984). This pattern is particularly characteristic for continental flood basalts (Thompson et al., 1984) and for subduction-related oceanic basalts (Wood et al., 1979; Pearce, 1982). Considering Table 2 and the high Sr<sub>i</sub> ratios (Alibert, this volume), the striking similarity with continental flood basalts is evident. Continental flood basalts typically

have high Ba and low Nb concentrations (Dupuy and Dostal, 1984), which similarly indicate subduction-related trace element patterns. Lightfoot and Hawkesworth (1988) emphasized the particular relationship between continental flood basalts and T-MORB. We therefore infer a source that contributes Ba and Th and retains the HFSE, especially Nb and Ta. These characteristics are typical for subduction-related arc basalts (Wood et al., 1979; Pearce 1982), the source of which retains HFSE as a result of refractory phases stable under high pH<sub>2</sub>O and pO<sub>2</sub>. This source is addressed as old, subducted, and partially remelted oceanic crust (Wood et al., 1979; Pearce, 1982; Hofmann and White, 1982; Thompson et al., 1984). After dehydration, partial melts from this "old" recycled oceanic crust, now a mantle section, still bear N-MORB signatures. When partial melts with MORB compositions from this deep reservoir rise, they vein the overlying mantle segment and interact with it. Interaction of rising basaltic magma with the overlying, thick mantle lherzolite may lead to HFSE and HREE depletion of the resulting magma due to incorporation of these elements into the refractory mantle mineral assemblage (olivine, orthopyroxene, spinel) with high crystal/liquid distribution coefficients (Kelemen et al. 1990). The resulting magma is depleted in HFSE, Cr, Ni, which are retained in the refractory mineral assemblage, and enriched in LREE and large ion lithophile elements (Kelemen et al. 1990), except for K and Rb, which may have escaped during former dehydration of the inferred downgoing slab.

It is concluded that the Site 738 basalts are derived from a veined upper mantle as proposed for the origin of T-MORB from the Southwest Indian Ridge (LeRoex et al., 1983). This veined upper mantle developed from interaction of basaltic liquids, derived from dehydrated, recycled oceanic crust underneath, with an overlying lherzolitic upper mantle. Slight differences in the degree of partial melting, and heterogeneity of the source are responsible for the observed slightly different magma batches. Ba and Th bows, LREE enrichment, HREE depletion, and Nb and Ta troughs (Fig. 16) can be explained by contamination of the source region with partial melts derived from dehydrated subducted oceanic(?) crust. This model needs thermal energy from a rising thermal plume (generation of large volumes of basaltic melts), which is the Kerguelen-Heard plume/hot spot. It does not need any continental crust material, nor a specific P-MORB/OIB magma.

The following model for the source region of Site 738 basalts is adopted from the above considerations:

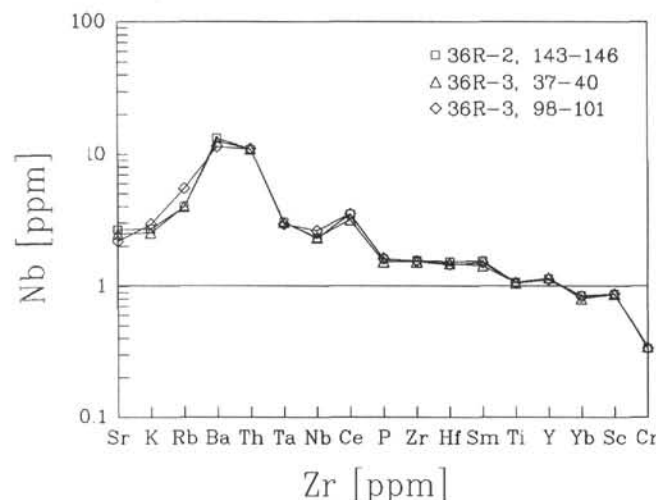


Figure 16. N-MORB-normalized element patterns of fresh Hole 738C samples. Normalization values from Pearce (1982).

1. Hot spot/plume-related heat transfer to the lithosphere is made responsible for the large amounts of partial melts (i.e., Kerguelen Plateau basalts).
  2. Interaction of rising basaltic liquids with overlying, thickened(?), lherzolitic upper mantle creates a veined upper mantle. Partial melting of this veined upper mantle is responsible for low HREE, Cr(?), Nb, and Ta concentrations (stored in refractory upper mantle mineral assemblage), high LREE, Ba, and Th concentrations (from the recycled basaltic crust wedge), and high Sr and Pb isotope values (cf. Alibert, this volume) of Site 738 basalts.

This model partially follows the suggestions from Hofmann and White (1982), where oceanic crust is subducted into the mantle, sinks to the lower mantle boundary, becomes heated, dehydrated, and partially melted. These partial melts have N/T-MORB(?) basaltic composition, migrate upward and vein the overlying lithosphere. The model also takes into account the suggestions of Kelemen et al. (1990), where basaltic liquid-upper mantle interaction is made responsible for HFSE and HREE depletions and LILE and LREE enrichments of arc-basaltic magma.

## CONCLUSIONS

1. The basaltic rocks of Site 738 of ODP Leg 119 belong to the plateau-forming stage (pre-Turonian) of southern Kerguelen Plateau formation. The aa-lava flows with basal and top breccias erupted under subaerial to shallow water, highly oxidizing conditions.
  2. The basement rocks are tholeiitic T-MORB with Zr/Nb around 17 and LREE enrichment, and high Ba and Th, and low Ta and Nb concentrations. CIPW norms, clinopyroxene phenocryst compositions (Ca-poor and Ca-rich), and plagioclase compositions (linear orthoclase increase) confirm the tholeiitic and transitional character of the basalts.
  3. The Site 738 T-MORB have undergone significant olivine (estimated about 8%) and some clinopyroxene fractionation (low Ni, medium Cr, and MgO concentrations) prior to eruption. Mixing between a more primitive, Mg-, Al-, Ti-, and Zr-rich, Fe-poor, slightly alkalic T-MORB-type magma, and a more evolved T/N-MORB-type tholeiitic magma with lower MgO, Al<sub>2</sub>O<sub>3</sub>, TiO<sub>2</sub>, and Zr and higher FeO can account for the observed variations in major and trace elements, and the crossing REE patterns.
  4. The source region is an enriched, veined upper mantle, bearing refractory phases which retain the HFSE, HREE, and especially Nb and Ta.
  5. Partial melts from an old, subducted, and recycled, oceanic(?) crustal component are the liquids veining the upper mantle, and are made responsible for the Ba and Th enrichment.
  6. The secondary mineral assemblage includes saponite, celadonite, montmorillonite (?), and Fe-oxides and Fe-hydroxides indicative of low-temperature seawater alteration (<170°C). Precipitation of calcite is due to terminal cold-seawater alteration.
  7. The alteration caused extensive oxidation and net gains in H<sub>2</sub>O, CO<sub>2</sub>, K<sub>2</sub>O, and Rb while CaO and V were released.

## ACKNOWLEDGMENTS

Research was funded by DFG (German Science Foundation) grants Schm 250/37-2/3 to H.-U. Schmincke, H. Niephaus, B. Schulz, and H.-J. Bernhard, all from Bochum University, helped with XRF and microprobe work. J. Dehn assisted with computer skills and B. Lehmann with drafting. To all of them we express our gratitude. Critical reviews by two anonymous reviewers helped to clarify results and are gratefully acknowledged.

## REFERENCES

- Andrews, A. J., 1979. On the effect of low-temperature seawater-basalt interaction on the distribution of sulfur in oceanic crust, Layer 2. *Earth Planet. Sci. Lett.*, 46:68–80.
- , 1980. Saponite and celadonite in layer 2 basalts, DSDP Leg 37. *Contrib. Mineral. Petrol.*, 73:323–340.
- Andrews, A. J., Barnett, R. L., MacClement, B.A.E., Fyfe, W. S., Morrison, G., MacRae, N. D., and Starkey, J., 1977. Zeolite facies metamorphism, geochemistry and some aspects of trace element redistribution in altered basalts of DSDP, Leg 37. In Aumento, F., Melson, W. G., et al., *Init. Repts. DSDP*, 37: Washington (U.S. Govt. Printing Office), 795–810.
- Baker, I., and Haggerty, S. E., 1967. The alteration of olivine in basaltic and Associated lavas. Part II: intermediate and low temperature alteration. *Contrib. Mineral. Petrol.*, 16:258–272.
- Barron, J., Larsen, B., et al., 1989. *Proc. ODP, Init. Repts.*, 119: College Station, TX (Ocean Drilling Program).
- Bassias, Y., Davies, H., Leclaire, L., and Weis, D., 1987. Basaltic basement and sedimentary rocks from the southern sector of the Kerguelan-Heard Plateau: new data and their Meso-Cenozoic paleogeographic and geodynamic implication. *Bull. Mus. Natl. Hist. Nat., Sect. C*, 9:367–403.
- Bednarz, U., and Schmincke, H.-U., 1989. Mass transfer during sub-seafloor alteration of the upper Troodos crust (Cyprus). *Contrib. Mineral. Petrol.*, 102:93–101.
- Bitschene, P. R., 1987. Mesozoischer und känozoischer, anorogener Magmatismus in Ostparaguay: Arbeiten zur Geologie und Petrologie zweier Alkaliprovinzen [Ph.D. dissertation]. Ruprecht-Karls-Univ., Heidelberg, FRG.
- Bitschene, P. R., Dehn, J., Mathis, J., Mehl, K., and Schmincke, H.-U., 1989. Die vulkano-tektonische Entwicklung im Indischen Ozean (Kerguelen Plateau, Broken Ridge, Ninetyeast Ridge): Ergebnisse der ODP Legs 119, 120 und 121. *Nachr. Dtsch. Geol. Ges.*, 41:12–13. (Abstract)
- Bitschene, P. R., Mehl, K. W., and Schmincke, H.-U., in press. Tephra layers from the Kerguelen Plateau, southern Indian Ocean (ODP Legs 119 and 120). In Schlich, R., Wise, S. W., Jr., et al., *Proc. ODP, Sci. Results*, 120: College Station, TX (Ocean Drilling Program).
- Brandon, A. D., and Goles, G. G., 1988. A Miocene subcontinental plume in the Pacific Northwest: geochemical evidence. *Earth Planet. Sci. Lett.*, 88:273–283.
- Davies, H. L., Sun, S.-S., Frey, F. A., Gautier, I., McCulloch, M. T., Price, R. C., Bassias, Y., Klootwijk, C. T., and Leclaire, L., 1990. Basalt basement from the Kerguelen Plateau and the trail of the Dupal plume. *Contrib. Mineral. Petrol.*, 103:457–469.
- Deer, W. A., Howie, R. A., and Zussman, J., 1978. *An Introduction to the Rock Forming Minerals*: New York (Longman).
- Donnelly, T. W., Thompson, G., and Salisbury, M. H., 1980. The chemistry of altered basalts at Site 417, DSDP Leg 51. In Donnelly, T., Francheteau, J., Bryan, W., Robinson, P., Flower, M., Salisbury, M., et al., *Init. Repts.*, 51, 52, 53 (Pt. 2): Washington (U.S. Govt. Printing Office), 1319–1330.
- Dosso, L., Bougault, H., Beuzart, P., Calvez, J.-Y., and Joron, J.-L., 1988. The geochemical structure of the South East Indian Ridge. *Earth Planet. Sci. Lett.*, 88:47–49.
- Duncan, A. R., Erlank, A. J., and Marsh, J. S., 1984. Regional geochemistry of the Karroo igneous province. In Erlank, A. J. (Ed.) *Petrogenesis of the Volcanic Rocks of the Karoo Province*. Spec. Publ. Geol. Soc. S. Afr., 13:355–388.
- Dupuy, C., and Dostal, J., 1984. Trace element geochemistry of some continental tholeiites. *Earth Planet. Sci. Lett.*, 67:61–69.
- Erlank, A. J., 1984. Petrogenesis of the volcanic rocks of the Karroo Province. *Geol. Soc. S. Afr. Spec. Publ.*, 13, 1–395.
- Frey, F. A., and Clague, D. A., 1983. Geochemistry of diverse basalt types from Loihi seamount, Hawaii: petrogenetic implications. *Earth Planet. Sci. Lett.*, 66:337–355.
- Gijbels, R., 1980. Reconstruction of the trace element distribution in the late Quaternary differentiated magma chambers of the Laacher See volcano (East Eifel). *Final Rep., EC contract 219-77 EGB, Univ. of Antwerpen*: 1–60.
- Hart, S. R., 1984. A large scale isotope anomaly in the Southern Hemisphere mantle. *Nature*, 309:753–757.
- Hertogen, J., and Gijbels, R., 1981. Instrumental neutron activation analysis of silicate rocks with low-energy photon detector. *Geochim. Cosmochim. Acta*, 56:61–82.
- Hofmann, A. W., and White, W. M., 1982. Mantle plumes from ancient oceanic crust. *Earth Planet. Sci. Lett.*, 27:421–436.
- Kelemen, P. B., Johnson, K.T.M., Kinzler, R. J., and Irving, A. J., 1990. High-field-strength element depletion in arc basalts due to mantle-magma interaction. *Nature*, 345:521–524.
- Klein, E. M., and Langmuir, C. H., 1988. Ocean ridge basalt chemistry, axial depth, crustal thickness and temperature variations in the mantle. *J. Geophys. Res.*, 92:8089–8115.
- Lawrence, J. R., 1980. Temperatures of formation of calcite veins in the basalts from Deep Sea Drilling Project Holes 417A and 417D. In Donnelly, T., Francheteau, J., et al., *Init. Repts. DSDP*, 51, 52, 53 (Pt. 2): Washington (U.S. Govt. Printing Office), 1183–1184.
- LeRoex, A. P., 1987. Source regions of mid-ocean ridge basalts: evidence for enrichment processes. In Menzies, M. A., and Hawkesworth, C. J. (Eds.), *Mantle Metasomatism*: London (Academic Press), 389–422.
- LeRoex, A. P., Dick, H.J.B., Erlank, A. J., Reid, A. M., Frey, F. A., and Hart, S. R., 1983. Geochemistry, mineralogy and petrogenesis of lavas erupted along the Southwest Indian Ridge between the Bouvet Triple Junction and 11 degrees east. *J. Petrol.*, 24:267–318.
- Lightfoot, P., and Hawkesworth, C., 1988. Origin of Deccan Trap lavas: evidence from combined trace element and Sr-, Nd- and Pb-isotope studies. *Earth Planet. Sci. Lett.*, 91:89–104.
- Loubet, M., Sassi, R., and Di Donato, G., 1988. Mantle heterogeneities: a combined isotope and trace element approach and evidence for recycled continental crust materials in some OIB sources. *Earth Planet. Sci. Lett.*, 89:299–315.
- MacDonald, G. A., and Katsura, T., 1964. Chemical composition of the volcanic rocks of Hawaiian lavas. *J. Petrol.*, 5: 82–133.
- Mahoney, J. J., Macdougall, J. D., Lugmair, G. W., and Gopalan, K., 1983. Kerguelen hotspot source for Rajmahal Traps and Ninetyeast Ridge? *Nature*, 303:385–389.
- Manson, B., and Moore, C. B., 1982. *Principles of Geochemistry* (4th ed.): New York (Wiley).
- Mantovani, M.S.M., Peate, D. W., and Hawkesworth, C. J., 1988. Geochemical stratigraphy of Parana continental flood basalts: a contribution from bore-hole samples. In Piccirillo, E. M., and Melfi, A. J. (Eds.), *The Mesozoic Flood Volcanism of the Parana Basin*: Sao Paulo (Inst. Astronom. e Geofis. Publ.), 15–24.
- Mehegan, J. M., and Robinson, P. T., 1982. Secondary mineralization and hydrothermal alteration in the Reydarfjordur Drill Core, Eastern Iceland. *J. Geophys. Res.*, 87:6511–6524.
- Mottl, M. J., and Holland, H. D., 1978. Chemical exchange during hydrothermal alteration of basalt by seawater. I. Experimental results for major and minor components of seawater. *Geochim. Cosmochim. Acta*, 42:1103–1115.
- Pearce, J. A., 1982. Trace elements characteristics of lavas from destructive plate boundaries. In Thorpe, R. S. (Ed.), *Andesites: Orogenic Andesites and Related Rocks*: New York (Wiley), 525–548.
- Rison, W., and Craig, H., 1983. Helium isotopes and mantle volatiles in Loihi seamount and Hawaiian island basalts and xenoliths. *Earth Planet. Sci. Lett.*, 66:407–426.
- Robinson, P. T., Flower, M.F.J., Schmincke, H.-U., and Ohnmacht, W., 1977. Low temperature alteration of oceanic basalts, DSDP Leg 37. In Aumento, F., Melson, W. G., et al., *Init. Repts. DSDP*, 37: Washington (U.S. Govt. Printing Office), 775–793.
- Schlich, R., Wise, S. W., Jr., et al., 1989. *Proc. ODP, Init. Repts.*, 120: College Station, TX (Ocean Drilling Program).
- Seyfried, W. E., Jr., and Bischoff, J. L., 1979. Low temperature basalt alteration by seawater: an experimental study at 70°C and 150°C. *Geochim. Cosmochim. Acta*, 43:1937–1947.
- Seyfried, W. E., Jr., Shanks, W. C., III, and Dibble, W. E., Jr., 1978. Clay mineral formation in DSDP Leg 34 basalt. *Earth Planet. Sci. Lett.*, 41:265–276.
- Staudigel, H., and Hart, S. R., 1983. Alteration of basaltic glass: mechanisms and significance of the oceanic crust-seawater budget. *Geochim. Cosmochim. Acta*, 47:337–350.
- Staudigel, H., Hart, S. R., and Richardson, S. H., 1981. Alteration of the oceanic crust: processes and timing. *Earth Planet. Sci. Lett.*, 62:311–327.
- Storey, M., Saunders, A. D., Tarney, J., Leaf, P., Thirlwall, M. F., Thompson, R. N., Menzies, M. A., and Marriner, G. F., 1988. Geochemical evidence for plume-mantle interactions beneath Kerguelen and Heard islands, Indian Ocean. *Nature*, 336:371–374.
- Sun, S.-S., and McDonough, W. F., 1989. Chemical and isotopic systematics of oceanic basalts: implications for mantle composition and processes. In Saunders, A. D., and Norry, M. J., (Eds.), *Magmatism in the Ocean Basins*. Geol. Soc. Spec. Publ. London, 42:313–345.

- Sun, S.-S., Nesbitt, R. W., and Sharaskin, A. Y., 1979. Geochemical characteristics of mid-ocean ridge basalts. *Earth Planet. Sci. Lett.*, 44:119–138.
- Thompson, R. N., Morrison, M. A., Hendry, G. L., and Parry, S. J., 1984. An assessment of the relative roles of crust and mantle in magma genesis: an elemental approach. *Philos. Trans. R. Soc. London*, 310:549–590.
- Viereck, L. G., Flower, M.F.J., Hertogen, J., Schmincke, H.-U., and Jenner, G. A., 1989. The genesis and significance of N-MORB sub-types. *Contrib. Mineral. Petrol.*, 102:112–126.
- Viereck, L. G., Griffin, B. J., Schmincke, H.-U., and Pritchard, R. G., 1982. Volcaniclastic rocks of the Reydarfjordur Drill Hole, eastern Iceland. 2. Alteration. *J. Geophys. Res.*, 87:6459–6476.
- Weaver, C. E., and Pollard, L. D., 1973. *The Chemistry of Clay Minerals. Developments in Sedimentology*, 15: Amsterdam (Elsevier).
- Weis, D., Bassias, Y., Gautier, I., and Mennesier, J.-P., 1989. DUPAL anomaly in existence 115 Ma ago: evidence from isotopic study of the Kerguelen Plateau (South Indian Ocean). *Geochim. Cosmochim. Acta*, 53:2125–2131.
- Wood, D. A., Joron, J. L., Treuil, M., Norry, M. J., and Tamey, J., 1979. Elemental and Sr isotope variations in basic lavas from Iceland and the surrounding ocean floor. *Contrib. Mineral. Petrol.*, 70:319–339.

Date of initial receipt: 2 January 1990

Date of acceptance: 7 August 1990

Ms 119B-130

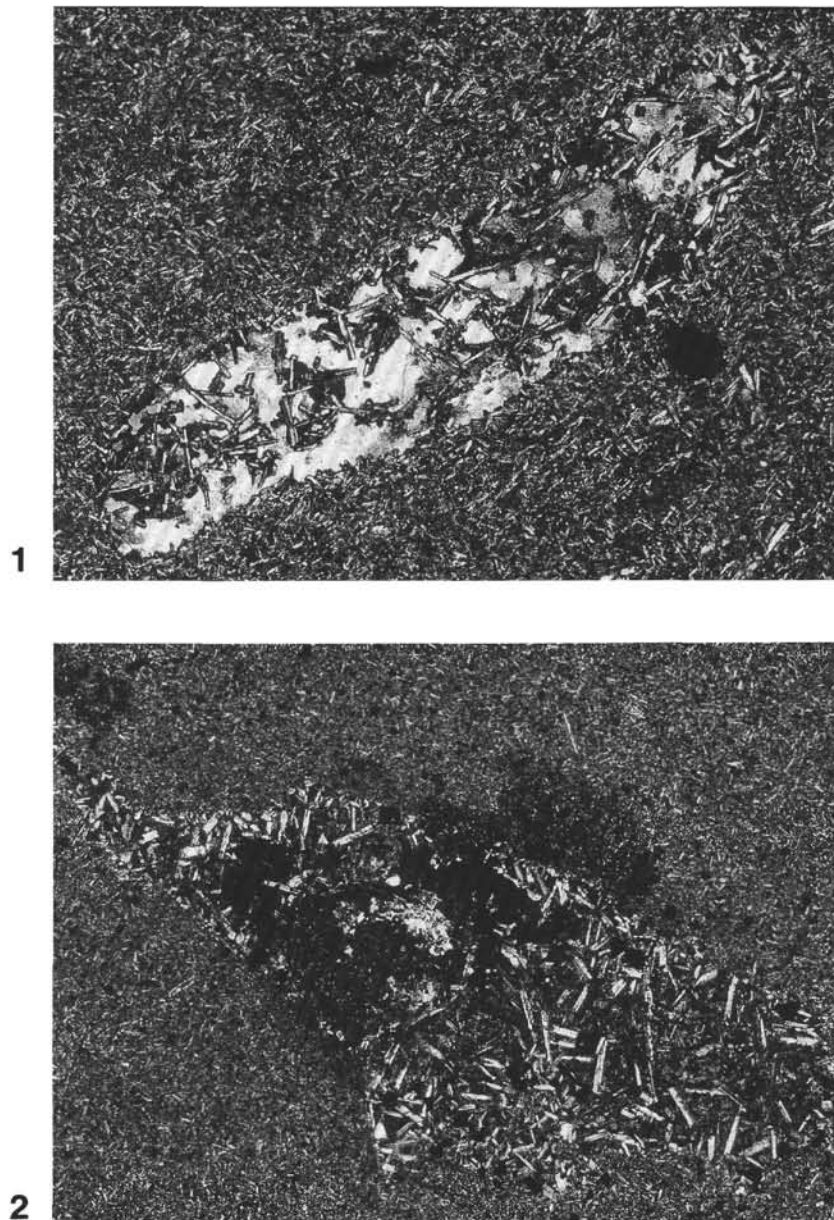


Plate 1. Pegmatoid "schlieren" in basalt. 1. Coarse plagioclase laths and clinopyroxene are rimmed by brown sheet silicates. Glassy matrix is replaced by calcite. Sample 119-738C-34R-4, 39-42 cm. Width of photo about 6 mm. Crossed nicols. 2. Coarse plagioclase laths and clinopyroxene lie in a groundmass replaced by K-feldspar. A vesicle (left of center) is filled by a dark brown sheet silicate, celadonite, and calcite. Sample 119-738C-33R-5, 30-32 cm. Width of photo about 9 mm. Crossed nicols.